International Journal of Nanomedicine

Dovepress
Taylor & Francis Group

Open Access Full Text Article

ORIGINAL RESEARCH

Anticancer Activity of Phospholipid-Dexibuprofen Conjugates Loaded in Nanostructured Lipid Carriers

Vaikunthavasan Thiruchenthooran[1], Marta Świtalska[2], Gabriela Maciejewska[3,4], Anna Palko-Łabuz[5], Lorena Bonilla-Vidal[6,7], Marta Espina[6,7], Maria Luisa Garcia[6,7], Joanna Wietrzyk[2], Eliana B Souto[8], Elena Sánchez-López[6,7], Anna Gliszczyńska[1]

[1]Department of Food Chemistry and Biocatalysis, Wrocław University of Environmental and Life Sciences, Wrocław, Poland; [2]Department of Experimental Oncology, Ludwik Hirszfeld Institute of Immunology and Experimental Therapy, Polish Academy of Sciences, Wrocław, Poland; [3]Central Laboratory of the Instrumental Analysis, Wrocław University of Technology, Wrocław, Poland; [4]Omics Research Center, Wrocław Medical University, Wrocław, Poland; [5]Department of Biophysics and Neuroscience, Wrocław Medical University, Wrocław, Poland; [6]Department of Pharmacy, Pharmaceutical Technology and Physical Chemistry, University of Barcelona, Barcelona, Spain; [7]Institute of Nanoscience and Nanotechnology (IN2UB), University of Barcelona, Barcelona, Spain; [8]UCD School of Chemical and Bioprocess Engineering, University College Dublin, Belfield, Dublin 4, D04 V1W8, Ireland

Correspondence: Anna Gliszczyńska, Email anna.gliszczynska@upwr.edu.pl; Elena Sánchez-López, Email esanchezlopez@ub.edu

Purpose: In our work, we focused on the development of nanostructured lipid carriers (NLCs) loaded with dexibuprofen (DXI) and their application for cancer therapy by proposing the binding of phospholipids with this non-steroidal anti-inflammatory drug (NSAID) to obtain new delivery systems.

Methods: We successfully synthesized seven conjugates with good yields, four of which are new, and have not been previously published in the literature. The structures of the obtained conjugates were confirmed and comparative in vitro studies of their antiproliferative activity were conducted, along with molecular modeling to assess their therapeutic potential.

Results: 1-DXI-2-hydroxy-*sn*-glycero-3-phosphocholine (DXI-LPC), 1-DXI-2-oleoyl-*sn*-glycero-3-phosphocholine (DXI-OA-PC) and 1-oleoyl-2-DXI-*sn*-glycero-3-phosphocholine (OA-DXI-PC) showed selectivity for cancer cells, influencing the cell cycle and inducing apoptosis. Encapsulation of heterosubstituted conjugates with increased lipophilic character in NLC resulted in DXI-PA-PC-NLC and DXI-OA-PC-NLC with favorable size (around 150 nm) and polydispersity index of 0.15, high encapsulation efficacy (above 99%), long-term stability, and modified release profile (51.4% and 48.9% of DXI released from DXI-PA-PC-NLC and DXI-OA-PC-NLC, respectively). Antiproliferative assays confirmed enhanced activity of synthesized products and their increased accumulation in cancer cells.

Conclusion: This study describes the synthesis of new conjugates of DXI and phospholipids and their nanotechnological formulations for potential use in cancer therapy.

Keywords: dexibuprofen, phospholipids, nanostructured lipid carrier, lipid nanoparticles, anticancer properties

Introduction

Since the release of the first nanodrug, Doxil®, by the American Food and Drug Administration (FDA) in 1995, nanotechnology has been progressively recognized as an essential instrument for creating innovative, more effective approaches and treatments against cancer.[1] The global nanomedicine market is currently valued at nearly $210 billions and is projected to grow significantly to $490 billions by 2032.[2] Currently, over 60 nanotherapeutics are available on the market, primarily for oncology, with more than 500 others in clinical trials (33% in Phase I and 21% in Phase II). Lipid nanoparticles account for the largest portion (33%) of all developed and available nanosystems.[3] The latest nanodrug successfully launched in 2018, Onpattro® (Patisiran), is based on lipid nanoparticles and is prescribed for managing polyneuropathy in individuals with hereditary transthyretin amyloidosis.[4] The current progress in nanotechnology is

Received: 26 January 2025
Accepted: 22 April 2025
Published: 30 May 2025

Graphical Abstract

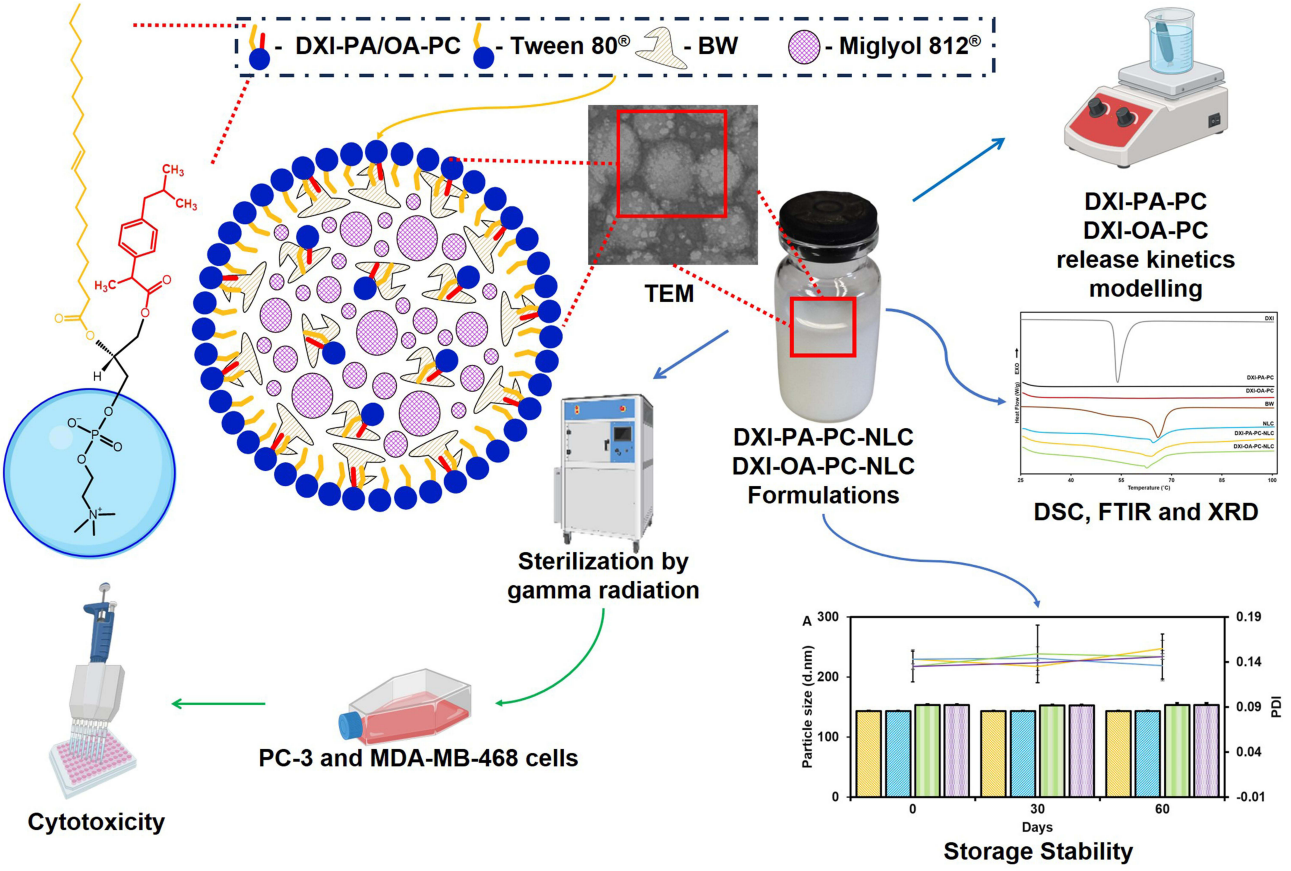

resulting in the creation of multifunctional nanoparticles that can deliver drugs precisely and efficiently, alongside enabling real-time imaging and monitoring of treatment responses, potentially crucial for future cancer therapies.

Lipid nanoparticles have many physical and biological advantages over other drug delivery systems. These particles are characterized by enhanced physicochemical stability and reduced toxicity, with the potential capacity to increase the efficacy of loaded drugs.[5,6] In developing effective cancer treatment technologies, lipid nanoparticles are safe and able to easily penetrate solid tumors, which is usually associated with high energy requirements. The small particle size allows them to accumulate at tumor sites, primarily through passive transport, by exploiting the increased permeability of blood vessels.[7] Moreover, they can be customized to exhibit selective action towards targeted tissues and cells, and to show modified release of the encapsulated drug.[1]

Nanoparticles loading lipid-drug conjugates (LDCs), obtained by linking the active biological molecule to a lipid compound (fatty acids, glycerides, or phospholipids), demonstrate significant potential. LDCs are gaining increasing interest in biomedical and pharmaceutical fields due to their capacity to improve the absorption and penetration of active ingredients across physiological membranes, thereby boosting the bioavailability and therapeutic effectiveness of these latter. Up to now, six lipid-drug conjugates have been approved by the European Medicines Agency (EMA) and by FDA for the treatment of conditions, like diabetes, depression, and schizophrenia.[1]

Phospholipids (PLs) have received considerable attention among lipid molecules that can be used to produce matrices for drug delivery. These molecules, which are components of cell membranes, are biocompatible and can enhance effectiveness of treatments for drugs with low bioavailability.[8,9] There are two strategies for conjugating drugs to PLs, namely, their binding to the phosphate group[10], and their attachment to the position *sn*-1 and/or *sn*-2 of the glycerol backbone.[11–13]

Dexibuprofen (DXI) is a widely used nonsteroidal anti-inflammatory drug (NSAID). It was introduced in Austria in 1994, and is categorized as a BCS class II drug, due to its low water solubility (0.0684 mg/mL), leading to limited bioavailability.[14] Its biological half-life ranges from 1 to 2 hours, and a 400 mg dose effectively treats inflammatory conditions.[15]

It has been shown that DXI and other NSAIDs can effectively inhibit tumorigenesis.[16–18] However, its application in the free form as chemopreventive and chemotherapeutic agent is not feasible owing to several unfavorable side effects linked to its anti-inflammatory action.[19] Therefore, in recent years, various delivery systems for DXI and other NSAIDs have been developed, such as self-emulsifying drug delivery systems,[20] chitosan nanoparticles,[21] nanocrystals,[22] nanoemulsions[23], solid lipid nanoparticles and nanostructured lipid carriers (NLCs).[24] Recently, DXI encapsulated in NLCs showed a significant increase in antiproliferative activity with selective action to cancer cells.[25] The adverse effects of NSAIDs on the gastrointestinal tract have also been reported to be attenuated with the use of phospholipid derivatives. PLs act as surfactants, forming a protective hydrophobic barrier on the mucus lining, thereby shielding gastrointestinal tissues.[26,27]

Based on this knowledge, we hypothesized that DXI conjugates with PLs would exhibit greater anticancer potential, selective action limited to cancer cells, improved physicochemical parameters, and favorable Absorption, Distribution, Metabolism and Elimination (ADME) properties. Furthermore, encapsulating these conjugates into NLCs allows biological effects to be achieved at a reduced drug dose. Consequently, two series of DXI phospholipid conjugates were synthesized, and their antitumor properties were assessed against representative types of the most common and aggressive cancers, such as leukemia (MV4-11), breast (MDA-MB-468 and MCF-7), lung (A-549), and prostate (PC-3) cancers, as well as in a non-tumorigenic human breast epithelial cell line (MCF-10A). The most potent DXI-phospholipid conjugates were chosen to study their molecular mechanisms of action and the most active conjugates were then selected for loading into NLC, followed by the assessment of the physicochemical properties of the obtained loaded particles and their efficacy and safety in selected cancer cell line models.

Materials and Methods

Chemicals and Reagents

Dexibuprofen (DXI), fatty acids (stearic and oleic), triethylamine (TEA), dibutyltin (IV) oxide (DBTO), 4-(*N, N*-dimethylamino)pyridine (DMAP), *N,N′*-dicyclohexylcarbodiimide (DCC), N,N-dimethylformamide (DMF), oxalyl chloride, celite® 110, Dowex® 50WX8 H^+ (ion-exchange resin), refined beeswax (BW), Tween® 80 (polysorbate 80), Nile red (NR), methanol, ethanol and acetonitrile of HPLC grade were purchased from Merck (Darmstadt, Germany). Glycero-3-phosphocholine (GPC) was ordered from Bachem AG (Bubendorf, Switzerland). Miglyol® 812 was acquired from Roig Farma SA (Terrassa, Spain), while indium (purity ≥99.95%) was supplied by Fluka (Buchs, Switzerland). Deionized water was prepared using a Millipore® Milli-Q® system (Merck KGaA) (Millipore, Darmstadt, Germany). Camptothecin (CPT) was purchased from (Sigma-Aldrich, Darmstadt, Germany). All other solvents were of analytical grade.

The formation of the conjugates was monitored using Thin-Layer Chromatography (TLC) on silica gel 60 F254 plates (0.2 mm aluminum plates with a fluorescent UV_{254} indicator(Merck, Darmstadt, Germany). Visualization required first staining with a 0.05% primulin solution prepared in a 4:1 (v/v) acetone:water mixture, following analysis under UV light at 365 nm. For column chromatography, Kieselgel 60 containing 0.1% Ca (230–400 mesh ASTM; Merck, Darmstadt, Germany) was employed, following a previously described protocol.[11] Spectroscopic data were recorded on a Bruker Advance II 600 MHz spectrometer (Bruker, Billerica, USA) following procedures outlined in a previously published work.[28]

Synthesis of DXI-Phospholipid Conjugates

1-DXI-2-lysophosphatidylcholine (DXI-LPC), 1-DXI-acyl-*sn*-glycero-3-phosphocholines and 1-acyl-2-DXI-*sn*-glycero-3-phosphocholines were synthesized according to previously reported procedures.[29,30] The obtained conjugates were purified using column chromatography as described before.[12]

 https://doi.org/10.2147/IJN.S512505

Molecular Modeling

The SPARTAN'18 software was used for the quantum calculations (Wavefunction, Inc., Irvine, CA, USA). The octanol-water partition coefficient (logP) and the topological polar surface area (TPSA) were determined using the Molinspiration software for online property calculations.

Production of DXI-NLC, DXI-PA-PC-NLC and DXI-OA-PC-NLC

NLC loaded with DXI and DXI-phospholipid conjugates (DXI-PA-PC and DXI-OA-PC) were produced using the hot high-pressure homogenization method.[25] As the lipid matrix, beeswax (BW) and Miglyol® 812 were used. For the loading of the particles, free DXI or each of the conjugates (DXI-PA-PC, and DXI-OA-PC) was dissolved in the melted lipid phase and preheated at 85 °C in a water bath for 30 min. After this time, an aqueous solution of Tween® 80 was added to the lipid phase, and the mixture was then homogenized under high shear using a Ultra-Turrax® T10 basic (IKA, Staufen, Germany) at 8000 rpm for 30s. The resulting emulsion was immediately exposed to three homogenization cycles (Pressure cell homogenizer-FPG12800, Stansted Fluid Power, Essex, UK) at a pressure of 11,603 psi and a temperature of 85 °C. All freshly prepared nanoemulsions were then allowed to settle at room temperature for 12 h for the recrystallization of the lipids to obtain NLC before further analysis. Empty NLC were produced in the same manner, but without the addition of any drug to the lipids.

Nile Red (NR) was used for labeling by preparing formulations following the procedure described above with the addition of 0.04% (w/w) of Nile Red (NR) to the formulation (DXI-NLC-NR, DXI-PA-PC-NLC-NR, and DXI-OA-PC-NLC-NR).[31]

Physicochemical Parameters

Dynamic light scattering (or photon correlation spectroscopy) was used to measure the hydrodynamic mean diameter (Z_{av}) and polydispersity index (PDI) of the obtained NLC. Their surface electrical charge was analyzed using laser-Doppler electrophoresis (Zetasizer Nano ZS Malvern Instruments). Samples were diluted with Milli-Q water 1:10 to avoid multi-scattering.[32,33] All measurements were conducted at 25 °C in triplicate.

Encapsulation Efficiency

Encapsulation efficacy (%EE) of DXI-PA-PC and DXI-OA-PC in NLC was quantified indirectly by ultrafiltration-centrifugation using 100 kDa ultrafilters (Merck KGaA, Darmstadt, Germany) to measure the free drug and applying Equation 1.

$$\%EE = \frac{(\text{Total initial amount of drug} - \text{Non-encapsulated drug})}{\text{Total initial amount of drug}} \times 100 \quad (1)$$

The formulations were diluted and filtered through centrifugation at 14000 rpm for 15 min (Mikro 22 Microliter Centrifuge, Germany). The supernatant, containing non-encapsulated DXI-PA-PC or DXI-OA-PC, was analyzed using a RP-HPLC system (Waters™, Milford, MA, USA) equipped with a Waters™ 2996 photodiode array detector, set to a wavelength of 220 nm. The mobile phase consisted of 0.05% orthophosphoric acid, acetonitrile, and methanol in a 5:15:80 (v/v) ratio, with a flow rate of 1 mL/min. Separation was carried out using a Kromasil® C18 column (5 µm × 4.6 mm × 150 mm) (Nouryon, Amsterdam, The Netherlands) at 25 °C, with an injection volume of 20 µL. Chromatograms were analyzed using Empower 3® software (Waters™, Milford, MA, USA). All measurements were performed in triplicate.

Interaction Studies

Transmission Electron Microscopy

Nanoformulations were subjected to the morphological analysis by Transmission Electron Microscopy (TEM) (JEOL 1010 transmission electron microscope, JEOL, Massachusetts, USA) after being diluted with Milli-Q water in a 1:5 ratio, and added with 2% of uranyl acetate to enhance contrast. Copper grids were activated with UV light and the samples were then applied to the grid surface.

Differential Scanning Calorimetry

DSC measurements of DXI, DXI-PA-PC, DXI-OA-PC, BW, empty NLC, and the fabricated DXI-PA-PC-NLC and DXI-OA-PC-NLC were taken in Mettler-Toledo, Barcelona, Spain). Calorimetric curves were obtained under nitrogen flow at a heating rate of 10 °C/min in the range of 10–100 °C. All the samples were accurately weighed in aluminum pans using a Mettler M3 microbalance (Greifensee, Switzerland). An identical empty aluminum pan was used as reference. A comparable indium pan was used to calibrate the calorimetric apparatus.

X-Ray Diffraction

The evaluation of crystallinity of DXI, DXI-PA-PC, DXI-OA-PC, BW, empty NLC, and the fabricated DXI-PA-PC-NLC and DXI-OA-PC-NLC was done by X-ray diffraction (XRD) (PANalytical's X-ray diffractometer, Almelo, Netherlands) using CuKα radiation (λ = 1.5418 Å, 45 kV, 40 mA) in the range (2θ) of 2°-60°.

Fourier Transform Infrared Spectroscopy

The absorption spectra DXI, DXI-PA-PC, DXI-OA-PC, BW, empty NLC, and the fabricated DXI-PA-PC-NLC and DXI-OA-PC-NLC were measured using a Thermo Scientific Nicolet iZ10 spectrophotometer, which featured an ATR diamond crystal and a DTGS detector (Barcelona, Spain). The scans covered a spectral range from 521–4000 cm^{-1}.[34]

Stability Studies

DXI-PA-PC-NLC and DXI-OA-PC-NLC were kept at two distinct temperatures (4 °C and 25 °C) for a period of two months. To assess the stability of the formulations, the Z_{av}, PDI, and ZP parameters were monitored over time.

Gamma Radiation

The prepared NLC formulations were sterilized through gamma irradiation (25 kGy of ^{60}Co) provided by Aragogamma (Barcelona, Spain). The impact of ionizing radiation on the NLC was evaluated by analyzing changes in the Z_{av}, PDI, ZP, and %EE.

In vitro Release Experiments

In vitro release of DXI-PA-PC and DXI-OA-PC from NLC formulations was determined by direct dialysis as explained elsewhere.[35] The diffusion experiment was performed using a 0.5 mL dialysis cassette (10K MWCO, Slide-A-Lyzer™, Thermo Scientific, Waltham, MA, USA) as the donor compartment. The acceptor compartment consisted of water-jacketed glass cells containing a release medium composed of ethanol and PBS (pH 7.4) in a 50:50 (v/v) ratio, maintained at a constant temperature of 37 °C under magnetic stirring. At specific time intervals, 400 µL of the release medium was withdrawn and replaced with an equivalent amount of freshly prepared medium. The collected samples were analyzed using RP-HPLC. The release profiles of DXI-PA-PC and DXI-OA-PC were plotted using GraphPad Prism 8.0 and fitted to standard biopharmaceutical models, as described previously.[36]

Biological Studies

Cell Lines

All cell lines were cultured at the Hirszfeld Institute of Immunology and Experimental Therapy (IIET PAS) in Wroclaw, Poland. The MV4-11 cell line, representing human biphenotypic B myelomonocytic leukemia, and the MCF-10A normal breast epithelial cell line were sourced from the ATCC (Manassas, Virginia, USA). Human non-small cell lung cancer (A-549), prostate cancer (PC-3), and breast cancer (MCF-7) cell lines were acquired from European Collection of Authenticated Cell Cultures (ECACC, Wiltshire, UK), while the MDA-MB-468 breast cancer cell line originated from the Leibniz Institute DSMZ (Leibniz, Germany).

MV4-11, PC-3, and MDA-MB-468 cells were cultured in RPMI 1640 medium (IIET PAS, Poland) with 1.0 mM sodium pyruvate (only MV4-11) 10% (MV4-11) or 20% (MDA-MB-468) fetal bovine serum (FBS) (all from Sigma-Aldrich, Darmstadt, Germany). A549 cells were maintained in RPMI 1640+Opti-MEM (1:1) (IIET PAS, Poland and Gibco, UK) supplemented with 5% FBS (Merck, Germany). The MCF-7 cells were grown in Eagle's medium

supplemented with insulin (8 μg/mL) and 1% MEM non-essential amino acids (Merck, Germany). MCF-10A cells were cultured in the HAM's F-12 medium (Corning) enriched with 10% Horse Serum (Gibco), EGFh (20 ng/mL), insulin (10 μg/mL), Hydrocortisone (0.5 μg/mL), and Cholera Toxin (0.05 mg/mL) from Vibrio cholerae (all from Merck, Germany). Cells were grown at 37 °C with 5% CO_2 humidified atmosphere and media were supplemented with L-glutamine (2 mM), penicillin (100 Units/mL) (Polfa Tarchomin S.A., Poland), and streptomycin (100 μg/mL) (Merck, Germany).

Determination of Antiproliferative Activity

The cytotoxicity of free DXI, its conjugates with phospholipids, and nanoformulations, was tested on five cancer cell lines (MV4-11, A549, PC-3, MDA-MB-468, and MCF-7), and on non-tumorigenic MCF-10A cell line used as a control. Cells were seeded into 96-well plates at specific densities 24 hours before exposure to the test compounds. DXI and its conjugates were tested at 5, 25, 125, and 625 μM, while the nanoformulations were tested at 4, 20, 100, and 500 μM, based on the encapsulated DXI-conjugates' concentration (1.5 mg/mL).

The cytotoxicity was evaluated after 24, 48, and 72 hours using the MTT assay for MV4-11, and the SRB assay for the remaining cell lines.[12] IC50 values were determined using Prolab-3 and Cheburator 0.4 software,[37] with results presented as mean ± SD. Each experiment was performed in triplicate, with three to five independent repetitions.

Cell Cycle Analysis

MV4-11 and MDA-MB-468 cells were seeded into 6-well plates (Sarstedt, Nümbrecht, Germany) at densities of 3×10^5 cells/well or 1.2×10^5 cells/well, respectively, to a final volume of 4 mL per well. The cells were exposed for 72 hours to the test compounds at concentrations about its 1.5×IC50 (DXI-LPC at 9 μM (MV4-11) or 4.5 μM (MDA-MB-468), DXI-OA-PC and OA-DXI-PC at 80 μM (MV4-11) or 150 μM (MDA-MB-468)). After incubation, 1×10^6 cells were collected, washed twice with cold PBS, and fixed in 70% ethanol at −20 °C for 24 hours. After fixation, the cells were washed twice with PBS and incubated for 1 hour with RNAse (8 μg/mL; Fermentas GmbH, Leon-Rot, Germany) at 37 °C, followed by staining with propidium iodide (50 μg/mL; Merck, Darmstadt, Germany) for 30 minutes at 4 °C. The DNA content of the cells was analyzed using a BD LSRFortessa cytometer (BD Biosciences, San Jose, CA, USA). Each compound was tested in triplicate at each concentration, and the data were processed using Flowing software 2.5.1 (Cell Imaging Core, Turku Centre for Biotechnology, University of Turku Åbo Akademi University, Finland).

Apoptosis Determination by Annexin V Staining

MV4-11 and MDA-MB-468 cells were seeded in 24-well plates (Sarstedt, Nümbrecht, Germany) at densities of 1×10^5 or 0.4×10^5 cells/well, respectively, to a final volume of 2 mL of culture medium. Cells were ecposed to the test compounds for 72 hours at concentrations of its 1.5×IC50 (DXI-LPC (9 μM (MV4-11) or 4.5 μM (MDA-MB-468), DXI-OA-PC and OA-DXI-PC at 80 μM (MV4-11) or 150 μM (MDA-MB-468)). After incubation the cells were collected and 2×10^5 cells were washed twice with PBS and suspended in 100 μL of buffer (Hepes buffer: 10 mM HEPES/NaOH, pH 7.4, 150 mM NaCl, 5 mM KCl, 1 mM $MgCl_2$, 1.8 mM $CaCl_2$, (IIET, Wrocław, Poland)with 4 μL of 2 μg/mL APC-Annexin V (BD Pharmingen, NJ, USA). Following a 15 minutes incubation in the dark at room temperature, propidium iodide solution was added to a final concentration of 4 μg/mL before analysis. Flow cytometry data acquisition was conducted using a BD LSRFortessa cytometer (BD Biosciences, NJ, USA). Each compound concentration was independently tested at least three times. The results were analyzed using Flowing software 2.5.1 (Turku, Finland). Results are presented in a two-color dot plot format with APC-Annexin V (AnV) versus propidium iodide (PI). Cells were categorized as follows: double-negative cells were considered live cells, PI-/AnV+ cells represented early apoptotic cells, PI+/AnV+ were classified as late apoptotic, and PI+/AnV- were categorized as necrotic cells. Each compound was tested in triplicate, with data averaged across three independent experiments.

Caspase-3/7 Activity Determination

MV4-11 and MDA-MB-468 cells were seeded in 48-well plates (Sarstedt, Nümbrecht, Germany) at a density of 0.5×10^5 or 0.2×10^5 cells/well, respectively, to a final volume of 1 mL of culture medium. The cells were exposed to the test compounds at concentrations of their 1.5×IC50 DXI-LPC at 9 μM (MV4-11) or 4.5 μM (MDA-MB-468) DXI-OA-PC

and OA-DXI-PC at 80 μM (MV4-11) or 150 μM (MDA-MB-468) for 24 or 72 hours. After incubation, cells were suspended in 50 μL of ice-cold lysis buffer (50 mM HEPES, 2 mM EDTA, 10% (w/v) sucrose, 10 mM DTT, 150 mM NaCl and 1% (v/v) Triton X-100, at pH 7.3 (IIET, Warsaw, Poland) and incubated for 30 min. at 4 °C. After the incubation, 40 μL of each sample was transferred to a white 96-well plate (Corning, NY, USA) containing 160 μL of the reaction buffer (20 mM HEPES, 1 mM EDTA, 10% sucrose, 10 mM DTT, 100 mM NaCl, 1 mM EDTA, 10 mM DTT, and 0.02% Triton X-100, at pH 7.3) (IIET, Wroclaw, Poland) with Ac-DEVD-ACC (final concentration 10 μM) fluorogenic substrate (λ_{ex} = 360 nm, λ_{em} = 460 nm). The increase of fluorescence was correlated with the caspase-3/7 levels and continuously recorded at 37 °C for 90 min using a Biotek Synergy H4 (Biokom, Warsaw, Poland). Compounds at each concentration were tested in duplicate in a single experiment, and each experiment was independently repeated at least thrice. The results were normalized to the number of cells in each well and are reported as the mean relative ± SD of caspase-3/7 activity compared to the untreated control sample.

Determination of Conjugates Accumulation in Cells by Flow Cytometry

Empty NLC formulation, DXI-NLC, and DXI-phospholipid conjugates-loaded NLC (DXI-PA-PC-NLC and DXI-OA-PC -NLC) were fluorescently labelled with Nile Red (NR) to assess their cellular uptake and accumulation. Prostate and breast cancer cells were treated with DXI-NLC-NR, DXI-PA-PC-NLC-NR, and DXI-OA-PC-NLC-NR at a concentration of 20 μM for varying durations (5, 15, 30 minutes, and 1, 2, and 4 hours). After treatment, the cells were washed with PBS and analyzed by flow cytometry. The mean fluorescence intensity of cells treated with NR-labeled formulations was measured using a BD LSRFortessa cytometer (BD Bioscience, San Jose, CA, USA) and subsequently analyzed with Flowing software 2.5.1 (Turku, Finland) Untreated cells were used as the control group.

Statistical Analysis

The Kruskal–Wallis test was used to compare two groups and to determine significant differences between treatments, using GraphPad Prism 7 software. A p-value of ≤ 0.05 was considered statistically significant.

Results and Discussion

Synthesis of Dexibuprofen-Phospholipid Conjugates

The chemical synthesis of the developed hybrid molecules aimed to produce two series of heterosubstituted phosphatidylcholines, with dexibuprofen positioned at either the *sn*-1 or *sn*-2 site of the phosphatidylcholine (PC) glycerol backbone (Schemes 1 and 2). The starting material, *sn*-glycero-3-phosphocholine (GPC), was commercially available. The optically pure form of GPC **(1)** was intentionally selected to create phosphatidylcholines with a natural (*R*)-

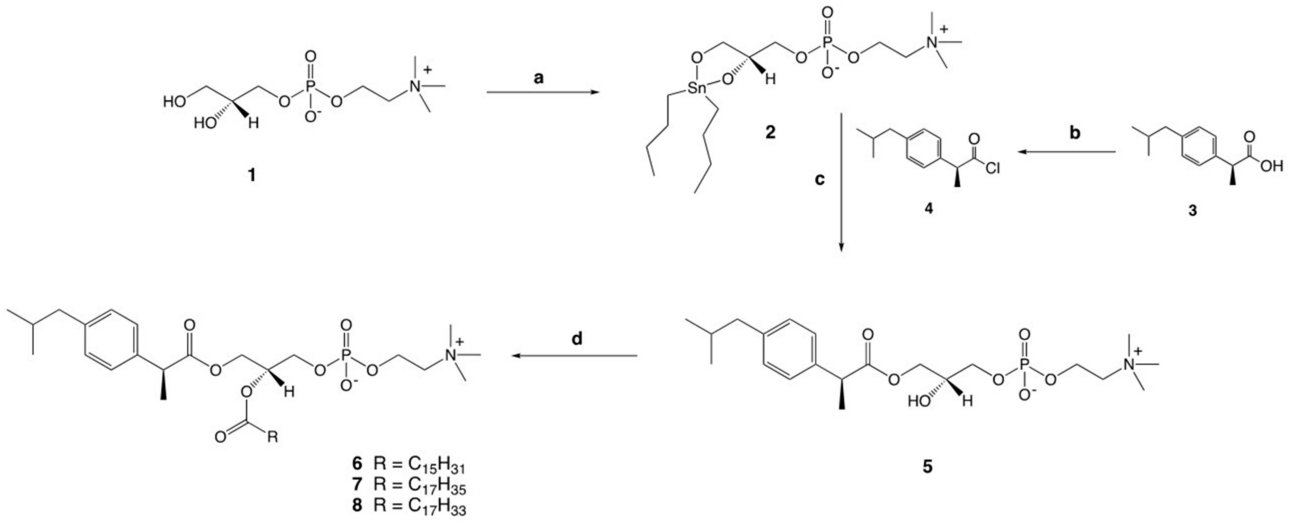

Scheme 1 Synthesis of 2-lysophosphatidylcholine **(5)** and phosphatidylcholines **(6–8)** structured with DXI. Reagents and conditions: a DBTO, 2-propanol, reflux, 1h; b oxalyl chloride, DMF, CH_2Cl_2; c TEA, rt, 1 h; d palmitic acid or stearic acid or oleic acid DMAP, DCC, 72 h.

https://doi.org/10.2147/IJN.S512505

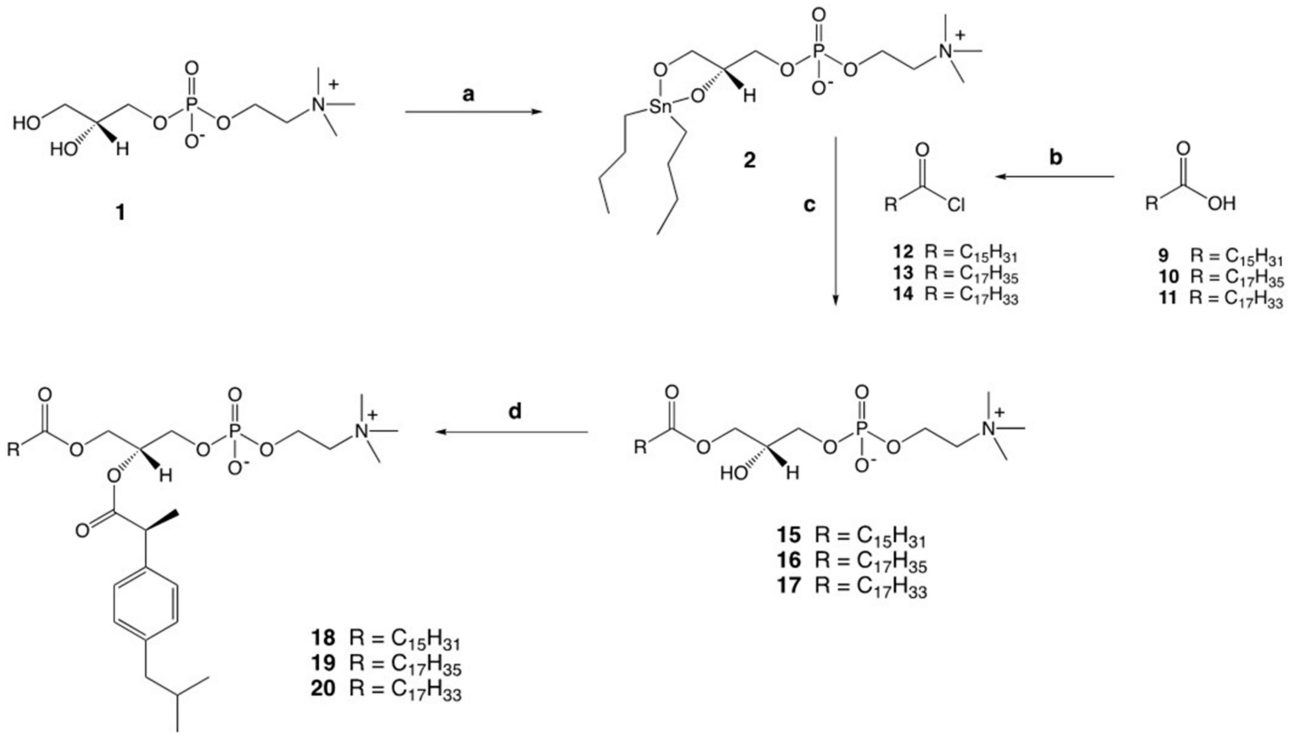

Scheme 2 Synthesis of phosphatidylcholines **(18–20)** structured with DXI. Reagents and conditions: a DBTO, 2-propanol, reflux, 1h; b oxalyl chloride, DMF, CH_2Cl_2; c TEA, rt, 1 h; d DXI, DMAP, DCC, 72 h.

configuration at the chiral center, allowing fatty acids at the *sn*-2 position to undergo PLA_2-catalyzed hydrolysis in the body.[38]

Conjugates with DXI at the *sn*-1 position were synthesized, as shown in Scheme 1. First, stannylene acetal (2) and chloride of DXI **(4)** were obtained according to a known procedure[30] and were then converted into 2-lysophosphatidylcholine (DXI-LPC) **(5)**, which was finally esterified with palmitic, stearic, or oleic acid, to the corresponding phosphatidylcholines **(6–8)** using the Steglich method.

In the next stage of the chemical synthesis of the DXI-PC conjugates, we followed the pathway depicted in Scheme 2. For the acylation of *sn*-1-palmitoyl/stearoyl or oleoyl lysophosphatidylcholine **(15–17)** by DXI, we used the same method as before, with *N,N'*-dicyclohexylcarbodiimide (DCC) in the presence of 4-(*N,N*-dimethylamino)pyridine (DMAP) as the catalyst, which resulted in the formation of the conjugates **(18–20)**.

The final compounds (**5–8** and **18–20**) were purified via column chromatography and achieved suitable yields ranging from 52% to 85%, with high purity (exceeding 99%), as determined by HPLC. Among the seven synthesized conjugates, four (**7, 8, 19, 20**) represent novel compounds not previously documented in the literature, while the remaining three (**5, 6**, and **18**) have been previously reported.[39] Structural confirmation of all obtained conjugates was established through spectroscopic data comparison with literature references for known compounds and, for new molecules, via nuclear magnetic resonance (NMR) analysis encompassing ^{1}H, ^{13}C, and ^{31}P nuclei, complemented by heteronuclear quantum correlation spectroscopy (HSQC), correlation spectroscopy (COSY), and electrospray ionization mass spectrometry (ESI-MS) analyses (Figure S1–S16). Spectroscopic data for all obtained products are presented in the Supplementary material.

Evaluation of Antitumoral Properties of Conjugates

To assess the cytotoxic properties of the synthesized conjugates **(5–8** and **18–20)**, the MTT assay was used on MV4-11 cells, and SRB assay on leukemia (MV4-11), lung (A549), prostate (PC-3), and breast (MDA-MB-468 and MCF-7) cell lines to measure cell viability. For these experiments, we chose the cell lines that represent the types of cancer for which the WHO report indicates the highest incidence and with the highest mortality rates.[40] In addition, we tested compounds

Table 1 The IC50 Doses of Dexibuprofen and Its Synthesized Phospholipid Derivatives Towards Cancer Cell Lines (MV4-11, A-549, PC-3, MDA-MB-468 and MCF-7) and Non-Tumorigenic Human Breast Epithelial Cell Line (MCF-10A), After 72 hours of Exposure

Compound	Cell Lines IC50 [μM]					
	MV4-11	A-549	PC-3	MDA-MB-468	MCF-7	MCF-10A
DXI	276.7 ± 101.0	349 ± 23.3	552.8 ± 50.1	n.a.	398.7 ± 13.9	435.2 ± 36
DXI-LPC	6.3 ± 0.9	42.7 ± 7.1	24.1 ± 4.6	3.2 ± 0.9	11.4 ± 0.5	9.7 ± 3.0
DXI-PA-PC	239.8 ± 71.7	139.7 ± 43.4	266.3 ± 27.7	283.7 ± 7.1	234.4 ± 32.1	340.2 ± 73.2
DXI-SA-PC	301.9 ± 11.7	n.a.	393.3 ± 72.3	316 ± 12.8	389.1 ± 23.8	n.a.
DXI-OA-PC	56.3 ± 0.6	57.3 ± 5.9	241.3 ± 22.9	106.9 ± 16.0	112.2 ± 16.2	228.5 ± 33.3
PA-DXI-PC	230.5 ± 56.1	267.5 ± 8.96	275.4 ± 9.7	284.6 ± 2.9	259 ± 15.0	352.3 ± 3.3
SA-DXI-PC	513.4 ± 102.1	n.a.	n.a	n.a.	530 ± 35.7	n.a.
OA-DXI-PC	54.7 ± 2.4	60.7 ± 2.8	225.2 ± 40.2	100.6 ± 12.3	111.5 ± 25.0	237.9 ± 12.9

Notes: Data are presented as the mean ± standard deviation (SD) calculated using the Prolab-3 system based on the Cheburator 0.4 software.[37] n.a.: not active in the concentration range (5–625 μM).

Abbreviations: DXI, dexibuprofen; DXI-LPC, dexibuprofenoyl-hydroxy-*sn*-glycero-3-phosphocholine; DXI-PA-PC, dexibuprofenoyl-palmitoyl-*sn*-glycero-3-phosphocholine; DXI-SA-PC, dexibuprofenoyl-stearoyl-*sn*-glycero-3-phosphocholine; DXI-OA-PC, dexibuprofenoyl-oleoyl-*sn*-glycero-3-phosphocholine; PA-DXI-PC, palmitoyl-dexibuprofenoyl-*sn*-glycero-3-phosphocholine; SA-DXI-PC, stearoyl-dexibuprofenoyl-*sn*-glycero-3-phosphocholine; OA-DXI-PC, oleoyl-dexibuprofenoyl-*sn*-glycero-3-phosphocholine; n.a., not active in the range concentration (5–625 μM).

against two type of breast cancer lines: in the MDA-MB-468, which does not express estrogen nor progesterone receptors and is E-cadherin negative and expresses mutant p53 (TNBC model), and in the MCF-7 characterized by the presence of estrogen, progesterone and glucocorticoid receptors. In the in vitro tests, the free DXI was used as a reference compound. To determine the level of selectivity of the conjugates, we also performed tests against the non-cancerous human breast epithelial cell line MCF-10A.

Table 1 depicts the obtained IC50 values. DXI-lysophosphatidylcholine (DXI-LPC) **(5)** and heterosubstituted phosphatidylcholines DXI-OA-PC **(8)** and OA-DXI-PC **(20)** exhibited significantly higher activity against almost all tested cancer cell lines in comparison to free DXI. Among all the tested products, DXI-LPC was the most effective at inhibiting the growth of leukemia cells at a dose that was 44-fold lower than that of non-conjugated DXI. DXI-LPC also exhibited activity against MDA-MB-468 cells (triple-negative breast cancer cell line) at 3.2 μM, whereas free DXI did not express any cytotoxic effect. In the MCF-7 cells (estrogen receptor-positive breast cancer cell line), the efficacy of DXI-LPC was 35 times greater than that of free DXI. Similarly, significantly higher activity was noted against prostate cancer PC-3 cells, where the IC50 value was 23 times lower compared of the non-conjugated DXI.

The results reveal that leukemia, lung and breast cancer cells were also sensitive to heterosubstituted phosphatidylcholines bearing an oleic acid moiety, thereby confirming the crucial role of unsaturated double bonds in the structure of the fatty acid acyl moieties to show cytotoxic effects. Prostate cancer cells (PC-3) were the most resistant among all the tested lines. DXI-oleoyl-*sn*-glycero-3-phosphocholine (DXI-OA-PC) **(8)** and oleoyl-DXI-*sn*-glycero-3-phosphocholine (OA-DXI-PC) **(20)** exhibited strong antiproliferative activity towards leukemia, lung and breast cancer cells with IC50 in the range 54.7–112.2 μM, which were 2 to 6-fold lower in comparison to non-conjugated DXI IC50. In contrast to free DXI, these compounds inhibited the growth of TNBC cells (MDA-MB-468) with IC50 values of approximately 101–107 μM.

In the evaluation of the anticancer potential of new compounds, it is important not only to confirm their capacity to eradicate cancer cells, but also to demonstrate their selectivity, which should be limited to cancer cells leading to their disruption. To assess the selectivity, a non-tumorigenic MCF-10A human mammary epithelial cell line was used as a control. The in vitro results obtained with the tested compounds on MCF-10A cells were used to calculate the selectivity index (SI). The SI values were determined by dividing the IC50 value obtained for the normal MCF-10A

Table 2 Selectivity Index (SI) of the Test Compounds, Obtained After 72h of Cell Exposure

Compound	Cell Lines/Calculated Selectivity Index (SI)				
	MV4-11	A549	PC-3	MDA-MB-468	MCF-7
DXI	1.57	1.25	0.79	-	1.12
DXI-LPC	1.54	0.23	0.40	3.03	0.85
DXI-PA-PC	1.42	2.43	1.28	1.2	1.45
DXI-SA-PC	-	-	-	-	-
DXI-OA-PC	4.06	3.99	0.95	2.14	2.04
PA-DXI-PC	1.53	1.32	1.28	1.24	1.36
SA-DXI-PC	-	-	-	-	-
OA-DXI-PC	4.35	3.92	1.06	2.36	2.13

Notes: SI = IC50 for normal cell line (MCF-10A)/ IC50 for respective tumor cell lines. An SI > 1.0 indicates a drug with greater efficacy against tumor cells than toxicity against normal cells.

Abbreviations: DXI, dexibuprofen; DXI-LPC,dexibuprofenoyl-hydroxy-*sn*-glycero-3-phosphocholine; DXI-PA-PC, dexibuprofenoyl-palmitoyl-*sn*-glycero-3-phosphocholine; DXI-SA-PC, dexibuprofenoyl-stearoyl-*sn*-glycero-3-phosphocholine; DXI-OA-PC, dexibuprofenoyl-oleoyl-*sn*-glycero-3-phosphocholine; PA-DXI-PC, palmitoyl-dexibuprofenoyl-*sn*-glycero-3-phosphocholine; SA-DXI-PC, stearoyl-dexibuprofenoyl-*sn*-glycero-3-phosphocholine; OA-DXI-PC, oleoyl-dexibuprofenoyl-*sn*-glycero-3-phosphocholine.

cell line by the IC50 value obtained for the specific tumor cell line under study (Table 2). For most phospholipid derivatives of DXI, the reported SI values were higher than those of the free DXI, which demonstrates the selectivity of the conjugates towards cancer cells. Only DXI-LPC showed no selectivity against A549, PC-3, and MCF-7 cells (SI < 1.0), whereas two derivatives bearing an oleic acid moiety (DXI-OA-PC and OA-DXI-PC) were the most active with similar high selectivity (except for PC-3 cells).

Effect of DXI-LPC, DXI-OA-PC and OA-DXI-PC on the Cell Cycle of MV4-11 and MDA-MB-468

The inhibitory effects of DXI-LPC, DXI-OA-PC, and OA-DXI-PC on cell cycle progression were evaluated in leukemia (MV4-11) and breast cancer (MDA-MB-468) cells. Following a 72-hours treatment, cell cycle analysis was performed using flow cytometry with nucleic acids stained with propidium iodide. The compound concentrations corresponded to 1.5 × IC50, as determined in previous cytotoxicity studies. The results were assessed by comparing the percentage of cells arrested at various stages of the cell cycle and those undergoing cell death (Figure 1A and B).

Cell cycle inhibition at the G0/G1 phase was identified by the presence of non-dividing cells or those that had completed mitosis, characterized by a single 2N genetic material content and a reduction in cells in the S phase (which includes those synthesizing genetic material, 4N). In MV4-11 cells (Figure 1A), DXI-LPC at cytotoxic doses induced cell death, while the heterosubstituted compounds, DXI-OA-PC and OA-DXI-PC, showed minimal cell cycle inhibitory activity. At 1×IC50, these compounds had no notable effect on the MV4-11 cell cycle. In MDA-MB-468 cells, all tested compounds reduced the number of cells in the G2/M phase. DXI-LPC arrested the cell cycle in the S phase, leading to cell death. DXI-OA-PC also resulted in cell death, while OA-DXI-PC caused cell cycle arrest in the G0/G1 phase, ultimately leading to cell death.

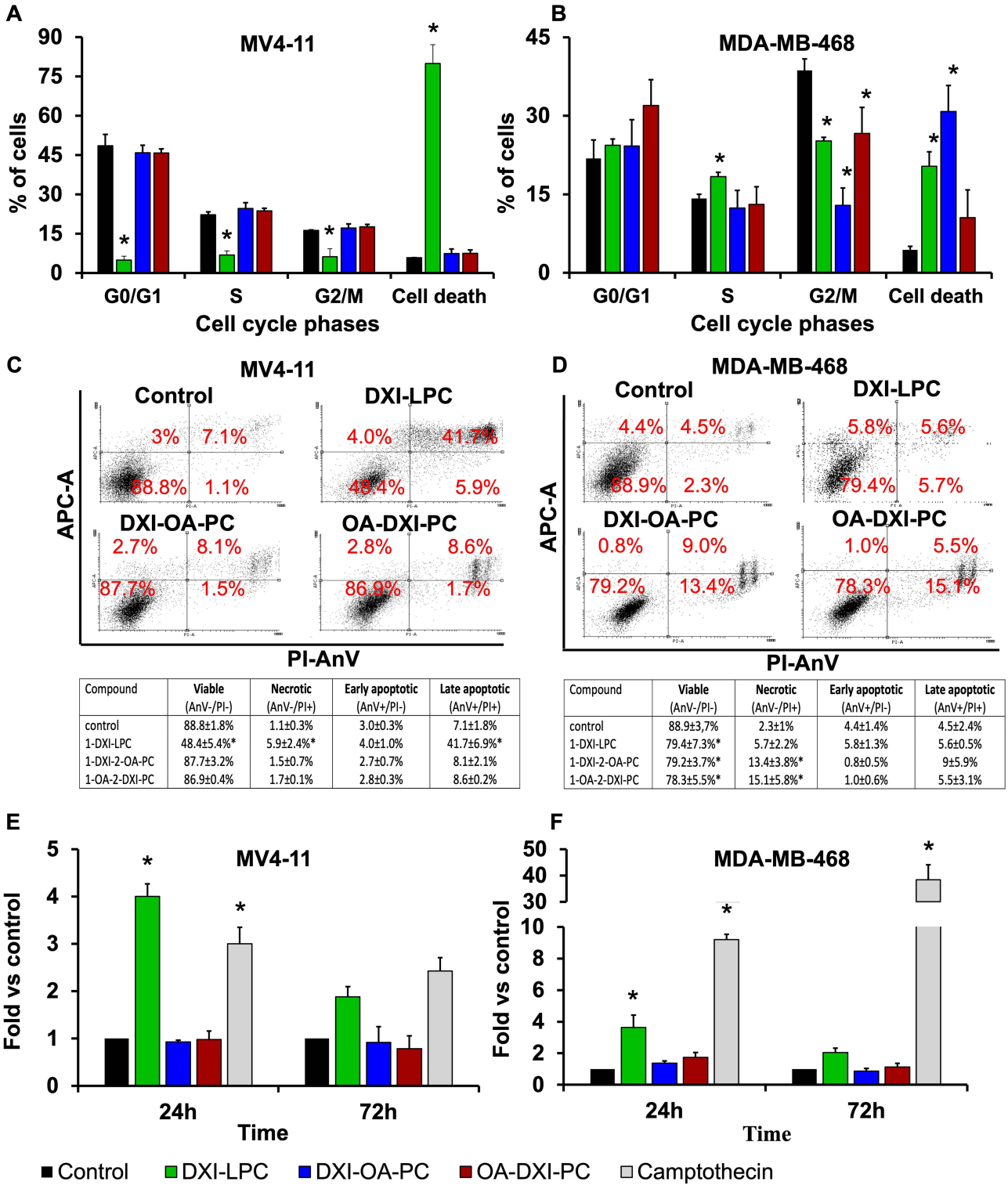

Compound	Viable (AnV-/PI-)	Necrotic (AnV-/PI+)	Early apoptotic (AnV+/PI-)	Late apoptotic (AnV+/PI+)
control	88.8±1.8%	1.1±0.3%	3.0±0.3%	7.1±1.8%
1-DXI-LPC	48.4±5.4%*	5.9±2.4%*	4.0±1.0%	41.7±6.9%*
1-DXI-2-OA-PC	87.7±3.2%	1.5±0.7%	2.7±0.7%	8.1±2.1%
1-OA-2-DXI-PC	86.9±0.4%	1.7±0.1%	2.8±0.3%	8.6±0.2%

Compound	Viable (AnV-/PI-)	Necrotic (AnV-/PI+)	Early apoptotic (AnV+/PI-)	Late apoptotic (AnV+/PI+)
control	88.9±3,7%	2.3±1%	4.4±1.4%	4.5±2.4%
1-DXI-LPC	79.4±7.3%*	5.7±2.2%	5.8±1.3%	5.6±0.5%
1-DXI-2-OA-PC	79.2±3.7%*	13.4±3.8%*	0.8±0.5%	9±5.9%
1-OA-2-DXI-PC	78.3±5.5%*	15.1±5.8%*	1.0±0.6%	5.5±3.1%

Figure 1 Cell cycle analysis (**A** and **B**) after 72 hours treatment, cell death analysis (**C** and **D**) and Caspase-3/7 expression analysis (**E** and **F**) of MV4-11 and MDA-MB-468 cells after 24- and 72-hours treatment. Treatment concentrations were DXI-LPC 9 μM (MV4-11) or 4.5 μM (MDA-MB-468), DXI-OA-PC and OA-DXI-PC 80 μM (MV4-11) or 150 μM (MDA-MB-468). *$p < 0.05$ in comparison to control cells, *Kruskal–Wallis* test, GraphPad Prism 7. AnV - Annexin V, PI - propidium iodide.

https://doi.org/10.2147/IJN.S512505

Effect of DXI-LPC, DXI-OA-PC and OA-DXI-PC on theCell Apoptosis of MV4-11 and MDA-MB-468

To identify the mode of cell death, a double staining method using annexin V antibody and propidium iodide was employed. The proportions of viable, early apoptotic, late apoptotic, and necrotic cells in MV4-11 and MDA-MB-468 cell lines are depicted in Figure 1C and D. In MV4-11 cells, treatment with DXI-LPC at 1.5 × IC50 led to a significant increase in apoptotic cells (AnV+/PI+), indicating apoptosis as the predominant form of cell death. Conversely, heterosubstituted phosphatidylcholines showed no apoptotic activity in MV4-11 cells, but induced necrosis (AnV-/PI+) in MDA-MB-468 cells.

Caspase-3/7 Activity Determination in MV4-11 and MDA-MB-468

The mechanism of action associated with apoptosis is the caspase cascade and activation of the apoptotic protein, caspase-3/7. The induction of caspase-3/7 activity was estimated using Ac-DEVD-ACC as the substrate after 24- and 72-hours incubation of leukemia (MV4-11) and breast cancer (MDA-MB-468) cell lines (Figure 1E and F). DXI-LPC significantly induced caspase-3/7 activity in both cell lines after 24 and 72 h of incubation, and the induction of caspase-3/7 was significantly lower. Its activity was higher than that of the positive control camptothecin (0.025 µg/mL) in MV4-11 cells, and this caspase-3/7 activity may be associated with the observed apoptosis and cell death induced by DXI-LPC (Figure 1). Heterosubstituted phosphatidylcholines did not induce caspase-3/7 activity after 24 or 72 h and had no impact on apoptosis.

Molecular Calculations

Quantum mechanical calculations were performed using the SPARTAN'18 application. In the first step for each investigated molecule, the conformer at the lowest energy was determined using the molecular mechanics/molecular force field (MM/MMFF) method. Full optimization of this conformer was performed using the Density Functional Method (DFT/B3LYP/6-31G* method). ΔE represents the "energy gap", which is the difference between E_{HOMO} (the energies of the highest occupied molecular orbital (EHOMO) and E_{LUMO} (the energy of the lowest unoccupied molecular orbital (ELUMO). The values of the absolute electronegativity (χ), chemical potential (μ), absolute hardness (η) and of the electrophilicity index (ω) were obtained using the following equations 2–4:[41–43]

$$\chi = -\mu = \frac{E_{HOMO} + E_{LUMO}}{2} \tag{2}$$

Table 3 Parameters Describing the Electronic Properties of Studied Molecules Calculated Using SPARTAN'18 Software

	E_{HOMO} (eV)	E_{LUMO} (eV)	ΔE (eV)	χ	η	ω	Dipole moment (Db)	PSA (Å^2)	Polarizability
DXI-LPC	−6.36	−0.05	6.31	3,21	3,16	1,63	16.42	80.040	77.31
DXI-PA-PC	−6.42	−0.24	6.18	3,33	3,09	1,79	19.95	89.933	101.73
DXI-SA-PC	−6.41	−0.23	6.18	3,32	3,09	1,78	18.87	89.037	104.72
DXI-OA-PC	−6.37	−0.14	6.23	3,26	3,12	1,7	16.97	88.301	104.34
PA-DXI-PC	−6.38	−0.35	6.03	3,37	3,02	1,88	18.07	88.446	101.75
SA-DXI-PC	−6.40	−0.32	6.08	3,36	3,04	1,86	18.79	88.891	104.75
OA-DXI-PC	−6.37	−0.45	5.92	3.41	2.96	1.96	19.59	88.236	104.48

Abbreviations: DXI, dexibuprofen; DXI-LPC,dexibuprofenoyl-hydroxy-*sn*-glycero-3-phosphocholine; DXI-PA-PC, dexibuprofenoyl-palmitoyl-*sn*-glycero-3-phosphocholine; DXI-SA-PC, dexibuprofenoyl-stearoyl-*sn*-glycero-3-phosphocholine; DXI-OA-PC, dexibuprofenoyl-oleoyl-*sn*-glycero-3-phosphocholine; PA-DXI-PC, palmitoyl-dexibuprofenoyl-*sn*-glycero-3-phosphocholine; SA-DXI-PC, stearoyl-dexibuprofenoyl-*sn*-glycero-3-phosphocholine; OA-DXI-PC, oleoyl-dexibuprofenoyl-*sn*-glycero-3-phosphocholine; E_{HOMO} and E_{LUMO}, HOMO and LUMO energy; ΔE, Energy gap; χ, absolute electronegativity; η, absolute hardness; ω, electrophilicity index; PSA, polar surface area.

$$\eta = \frac{E_{HOMO} - E_{LUMO}}{2} \quad (3)$$

$$\omega = \frac{\mu^2}{2\eta} \quad (4)$$

The descriptors characterizing the electronic properties of the studied molecules are listed in Table 3. The results of our calculations show that the conjugation of DXI with fatty acids increased the polar surface area of the molecules. However, the polar surface area (PSA) values obtained were less than 140 $Å^{2.}$ predicting the absorption of conjugates through biological barriers, and the possibility of their use for oral administration.[44]

All the studied compounds containing fatty acids (palmitic, stearic, or oleic) in the structure had lower ΔE and η values than DXI-LPC. The highest ΔE and η values for DXI-LPC indicate that this compound was the most stable among the studied derivatives, which may be related to its lower reactivity. The higher reactivity of the conjugates with fatty acids was also indicated by the higher values of χ, ω, dipole moment, and polarizability calculated for these molecules. χ refers to an atom's tendency to attract electrons, whereas ω expresses the tendency of electron acceptors to take up additional electronic charge from the surroundings. We confirmed that the presence of fatty acids in the structures of the compounds strengthened the electrophiles. In parallel, the higher polarizability indicates an increased tendency of the compounds to generate induced electric dipole moments during exposure to the electric field.

The calculations show that the position of DXI in the structure of the conjugate influences its stability. Derivatives substituted with DXI at *sn-2* position of phosphatidylcholine had lower ΔE and η values than derivatives containing DXI at *sn-1* position. Moreover, the values of χ, ω, dipole moment, and polarizability suggest that the molecules containing the drug at *sn-2* are more potent electrophiles than *sn-1* substituted derivatives and may show higher reactivity. In addition, considering the parameters obtained for conjugates substituted with DXI at *sn-2* position, we anticipate that compounds containing oleic acid may be the most promising in biological systems.

Preparation of DXI-phospholipid conjugates loaded Nanostructured Lipid Carriers

We hypothesize that the loading of DXI-phospholipid conjugates, with previously proven antiproliferative activity, into NLCs may increase the efficacy of the former in eradicating cancer cells by improving cellular uptake.

Heterosubstituted phosphatidylcholines were selected for encapsulation into NLCs owing to their lipophilic nature, which is essential to reach high EE%. Among the two types of synthesized heterosubstituted hybrid molecules, we selected those in which the drug was linked to the glycerol backbone of the phosphatidylcholine at the *sn*-1 position, whereas at the *sn*-2 position, an acyl fragment from a long-chain fatty acid was present. Under tumor cell conditions characterized by a high concentration of phospholipase A_2, this acyl fragment may be hydrolyzed to produce DXI-LPC, which exhibits even higher activity towards cancer cells than the heterosubstituted phosphatidylcholines. Despite the notably lower activity of the conjugates of palmitic acid compared to the derivatives of oleic acid, we decided to encapsulate both to investigate the impact of their loading into NLCs on enhancing the activity of biologically active compounds. Therefore, a previously optimized NLC formulation was used[25] to produce empty NLCs and NLCs loaded with either DXI-PA-PC or DXI-OA-PC (Table S1).

The empty NLCs exhibited a particle size of 156.3 nm with a PDI below 0.2. The DXI-PA-PC-NLC and DXI-OA-PC -NLC showed smaller particle sizes of 143.5 nm and 151.6 nm, respectively, with monomodal distributions and PDI values of 0.15. Both DXI-PA-PC-NLC and DXI-OA-PC-NLC showed negative ZP values of –16.1 mV and –13.5 mV, respectively. These ZP values were less negative than those of the empty NLC, likely due to the positively charged choline head group, which reduces the overall anionic charge (Table S1).

According to the literature, small particles with a diameter range of 50–300 nm have higher ability to be taken up by the cells.[45] Besides, interaction with cell membranes, internalization processes, opsonization, and stability within biological fluids are significantly influenced by the surface electrical charge of the particles.[46] Although it has been proven that positively charged nanoparticles can internalize tumor cells more effectively[47] (which possess a negative surface charge),[48] anionic nanoparticles are safer and showed reduced hepatic nonspecific uptake.[49–51]

Encapsulation Efficacy

The encapsulation efficiency (%EE) of both DXI-phospholipid conjugates was higher than 99% (Table S1). After incorporation into the *sn*-1 position of glycero-3-phosphocholine (GPC), DXI-LPC exhibited hydrophilic character, which was confirmed by the molecular calculations (negative logP value of DXI-LPC) (Table S2), whereas the lipophilicity of heterosubstituted phosphatidylcholines increased (Table S2) which influenced the encapsulation these conjugates into NLC.

Physicochemical Characterization of DXI-PA-PC-NLC and DXI-OA-PC-NLC

TEM analysis shows that the fabricated NLCs had a predominantly spherical shape and regular morphology, with no particle aggregation (Figure 2), regardless of the incorporation of DXI-phospholipid conjugates. It is well-known that nanosized dispersions of different shapes exhibit distinct immune responses.[52] Spherically shaped submicron-sized particles can bypass immune response-mediated clearance and can show a relatively higher half-life to passively target tumor cells over a longer time.[52–54] Fabricated nanoparticles with encapsulated NSAID (DXI-PA-PC-NLC and DXI-OA-PC-NLC) did not show particle fusion or aggregation, which may be due to their highly negative surface charge.[52,55]

Differential scanning calorimetry (DSC) was performed to evaluate the crystallinity and melting point of free drug (DXI), its phospholipid conjugates (DXI-PA-PC, DXI-OA-PC), bulk solid lipid (BW), empty NLC, and fabricated NLC formulations (DXI-PA-PC-NLC and DXI-OA-PC-NLC). The thermograms (Figure 2C) show the melting point of DXI at 53.6 °C, as reported in a previous work.[25] Due to their amorphous physical state, DXI-PA-PC and DXI-OA-PC did not show any melting phenomena.[56] The onset glass transition temperature (T_g) of BW was at 61.39 °C, whereas for empty NLC it was at 61.31 °C. Loading of DXI-PA-PC and DXI-OA-PC into NLCs resulted in further reduction of T_g and melting enthalpy down to T_g = 54.5 °C and ΔH = 57.5 J/g, and to T_g = 57.2 °C and ΔH = 57.5 J/g and ΔH = 56.9 J/g, respectively.

The X-ray diffraction (XRD) profile was performed to confirm the crystallinity of the conjugates in NLCs.[57] The obtained diffractograms are presented in Figure 2D. DXI exhibits several Bragg peaks that confirm its crystallinity.[58] The phospholipid conjugates presented an amorphous profile. The XRD pattern of BW shows two distinct Bragg peaks, one at 21.4° and other at 23.8°, corresponding to the diffraction of *n*-nonacosane ($C_{29}H_{60}$) and *n*-tricosane-*n*-pentacosane ($C_{25}H_{52}$), which are abundant in natural waxes.[59]

The diffractograms of DXI-PA-PC-NLC and DXI-OA-PC-NLC show the crystalline peaks of the beewax and do corroborate the results obtained by DSC[60], where no melting peak of DXI in the DXI-conjugates-loaded NLC was found. The lack of diffraction peaks does not necessarily mean that DXI-conjugates are not present in the sample; in the characterization of nanoparticle surfaces by XRD, it is commonly reported that drugs can be near the surface yet without signals in diffractograms.

ATR-FTIR analysis was conducted to assess the chemical interactions[61] and changes between the drug, surfactant, and lipid matrix components (Figure 2E). In the FTIR spectrum of DXI, vibrational bands at 2869–2952 cm^{-1} were identified as symmetric and asymmetric CH_2 stretching vibrations, while the characteristic band at 1701 cm^{-1} corresponded to carboxyl C=O stretching. Additional weak intensity bands appeared in the fingerprint region, associated with C-C stretching (1508, 1466, and 1417 cm^{-1}), C-O stretching (1282 cm^{-1}), and O-H bending (778 cm^{-1}). In the spectra of DXI-phospholipid conjugates, characteristic bands for C=O at 1729 cm^{-1} and carbonyl ester stretching at 1649 cm^{-1} were observed. In the fingerprint region, P=O stretching and P-O-C stretching bands of the phosphate group were evident at 1235 and 1070 cm^{-1}, respectively. These findings confirm the presence of DXI, oleic acid or palmitic acid at both positions of phosphatidylcholine (PC), supported by the absence of O-H bonds and the appearance of C=O and carbonyl ester bond vibrations. No new covalent bonds were detected in the DXI-phospholipid conjugates-loaded NLCs.

Storage Stability

The stability of DXI-PA-PC-NLC and DXI-OA-PC-NLC was assessed on day 1, and after 30 and 60 days of storage at two temperatures, 4 and 25 °C. For this purpose, the mean particle size, PDI, and ZP were measured, and the obtained results are summarized in Figure 3. As shown, the DXI-PA-PC-NLCs and DXI-OA-PC-NLCs maintained their

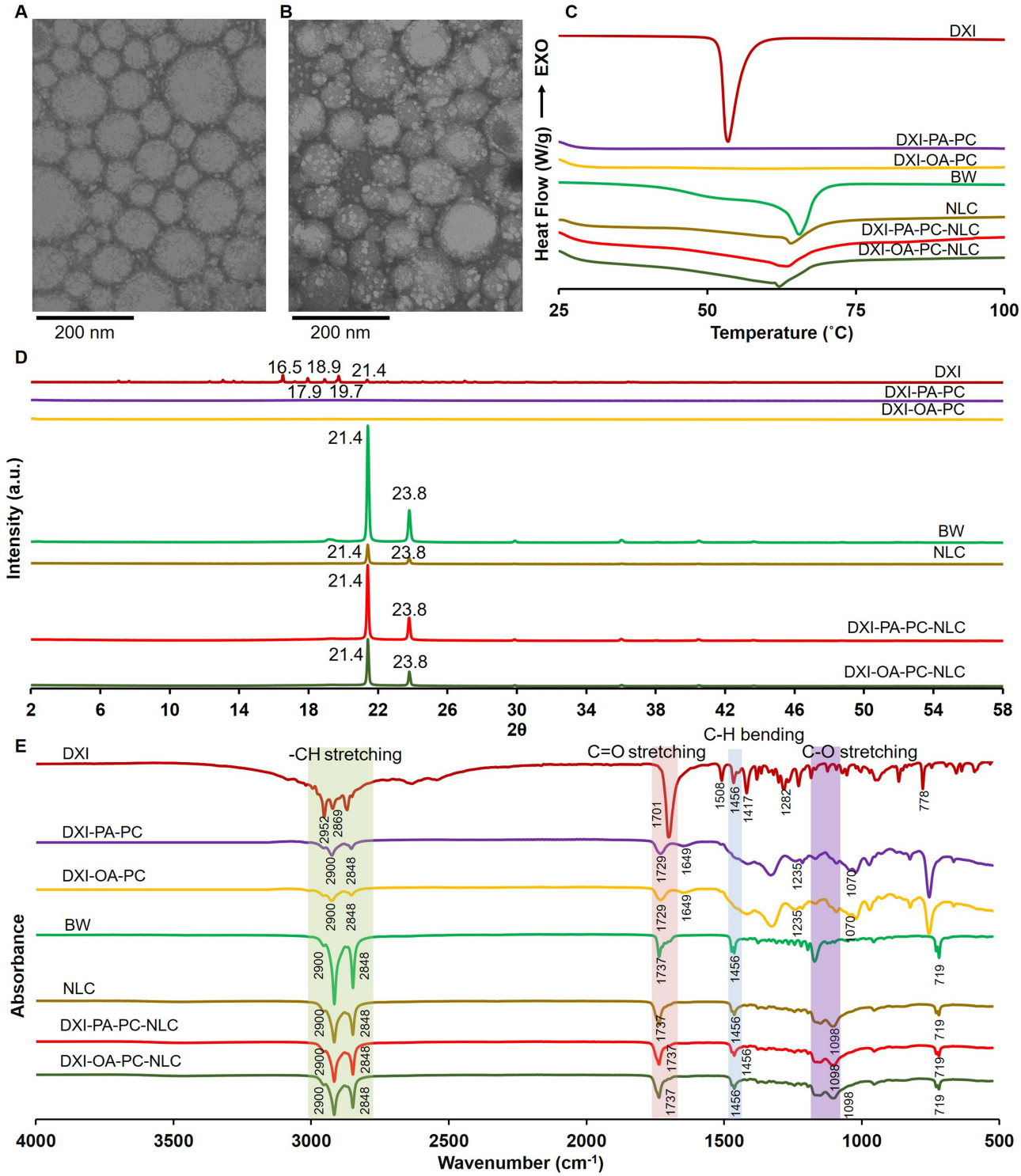

Figure 2 Morphological characterization using transmission electron microscopy of (**A**) DXI-PA-PC-NLC and (**B**) DXI-OA-PC-NLC, and characterization of nanocarriers using differential scanning calorimetry (**C**), X-ray diffraction (**D**) and Fourier transform infrared spectroscopy (**E**) of dexibuprofen (DXI), synthesized phospholipid-DXI conjugates (DXI-PA-PC and DXI-OA-PC), beeswax (BW), empty nanostructured lipid carriers (NLC) and conjugates-loaded NLC (DXI-PA-PC-NLC and DXI-OA-PC-NLC).

https://doi.org/10.2147/IJN.S512505

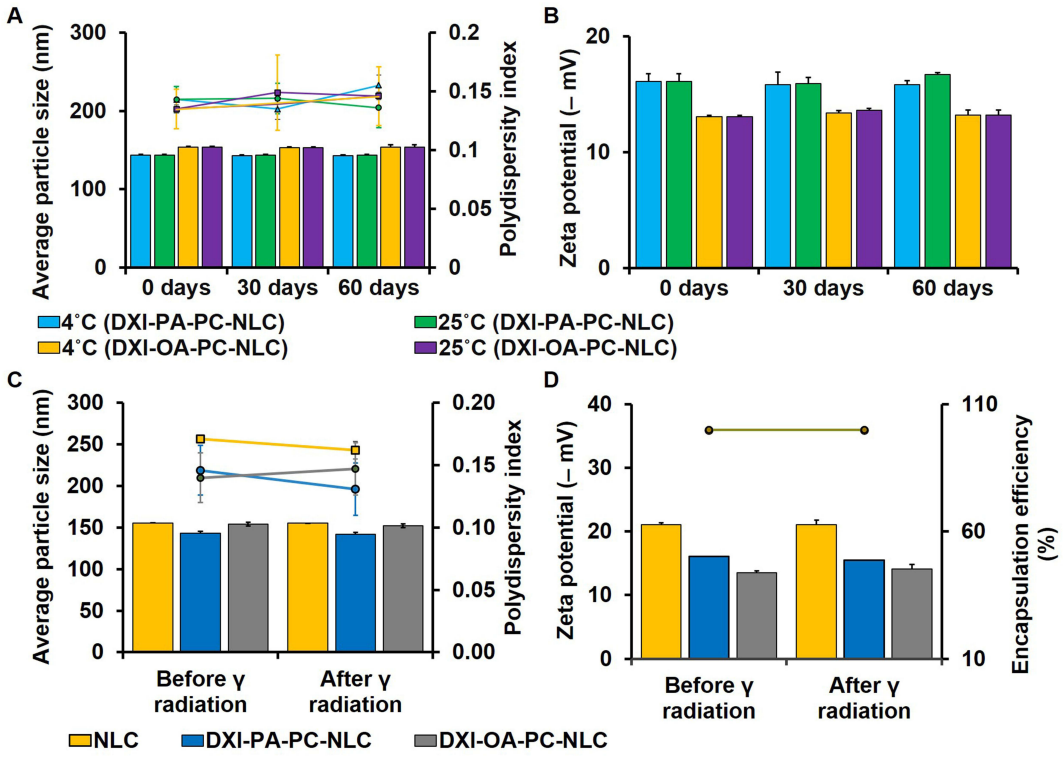

Figure 3 Stability of DXI-PA-PC-NLC and DXI-OA-PC-NLC during storage at two distinct temperatures (4 and 25 °C). (**A**) (bars), mean particle size; (**A**) (lines), polydispersity index (PDI); (**B**) zeta potential (ZP); Effect of gamma radiation on DXI-conjugates-loaded NLC on the particle size (**C**, bars), on the PDI (**C**, lines), on the ZP (**D**, bars) and on the encapsulation efficiency (EE%) (**D**, lines). Results are presented as mean ± SD, n = 3.

physicochemical properties when stored at both temperatures. The PDI values (Figure 3A) of all formulations were below 0.2 and showed no differences over the storage time at the two different temperatures. Similarly, ZP values (Figure 3B) of DXI-PA-PC-NLC and DXI-OA-PC-NLC (–16.2 ± 0.7 and –13.3 ± 0.8) did not show differences over storage time. Therefore, during the initial 60 days after preparation, both formulations showed suitable stability at 4 °C and 25 °C.[62] However it is known that, due to polymorphic transformations in their matrices, lipid nanoparticles can expel the loaded drug during storage[62]. However, during our experiments, we did not observe any physical changes, such as sedimentation or creaming, that could result from DXI expulsion from NLCs.

Effect of Gamma Radiation

The biopharmaceutical applications of nanoparticles require proper selection of a sterilization method. It is known from the literature that high-temperature sterilization methods may compromise the physicochemical properties of nanoparticles, whereas gamma irradiation constitutes an acceptable sterilization technique for pharmaceutical products.[55] DXI-PA-PC-NLC and DXI-OA-PC-NLC were exposed to 25 kGy of ^{60}Co source. The mean particle size, PDI, ZP, and %EE were evaluated before and after sterilization. Based on the results presented in Figure 3C and D, we confirmed that the particle size and ZP had no statistical deviation from their initial values, and the polydispersity remained below 0.2. Based on these results, gamma radiation was selected for sterilization of the final formulations prior to cell testing.

In vitro Release

The in vitro release of free DXI-conjugates and DXI-conjugates-loaded NLC was measured at 37 °C for 24 h. DXI in the form of phospholipid derivatives reached equilibrium after 10 h. For conjugates encapsulated in NLC, a slower release was obtained (51.4% and 48.9% for DXI-PA-PC-NLC and DXI-OA-PC-NLC, respectively). Moreover, DXI-PA-PC-NLC and DXI-OA-PC-NLC showed an initial burst release attributed to the presence of conjugates near the NLC surface, which initiates a fast release followed by a prolonged release of DXI-conjugates placed in the inner matrix of

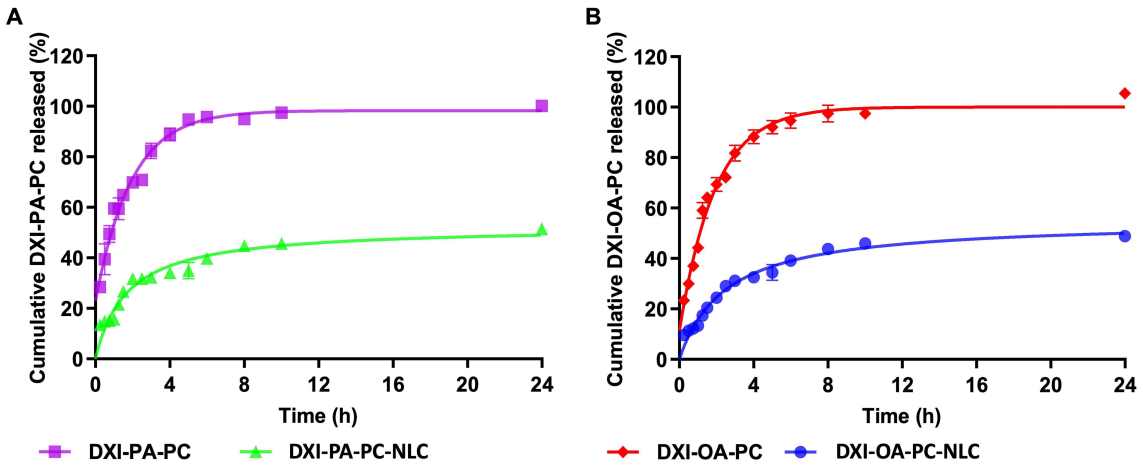

Figure 4 In vitro release profiles of (**A**) DXI-PA-PC and DXI-PA-PC-NLC, and of (**B**) DXI-OA-PC and DXI-OA-PC-NLC, pH 7.4 (mean ± SD, n = 3).

NLC.[54] In a previous study, DXI-NLC released ca. 73% of the loaded drug within the first 10 hours.[25] Conjugation of DXI with PC containing long-chain fatty acids (palmitic and oleic acids) led to the creation of drug derivatives with higher lipophilic properties, thus affecting the release profiles. The obtained release profiles were adjusted to kinetic models[36] and the outputs are listed in Table S3. The best adjustment for free DXI-conjugates was the first-order release, and that for DXI-conjugates-loaded NLC was the hyperbolic model. The profiles of free DXI-conjugates and DXI-conjugates-loaded NLC are shown in Figure 4A and B.

In vitro Anticancer Activity of Fabricated Formulations

The anticancer potential of DXI-PA-PC-NLC and DXI-OA-PC-NLC was assessed using an SRB assay on prostate (PC-3) and breast (MDA-MB-468) cancer cell lines (Table 4). NLCs loaded with DXI-PA-PC and DXI-OA-PC demonstrated significantly greater anticancer activity compared to the free drug and its conjugates (DXI-PA-PC and DXI-OA-PC). In PC-3 cells, after 72 hours of incubation, the IC50 value for free DXI was 552.8 µM (Table 1), while its conjugates DXI-PA-PC and DXI-OA-PC showed IC50 values of 266.3 µM and 241.3 µM, respectively. Encapsulation of these conjugates in NLCs enhanced their antiproliferative activity by 20- and 18-fold, reducing the IC50 to 12.7 µM for DXI-PA-PC-NLC and 12.9 µM for DXI-OA-PC-NLC (Table 4). In MDA-MB-468 cells, DXI-PA-PC exhibited an IC50 of 283.7 µM, and DXI-OA-PC demonstrated a stronger effect with an IC50 of 106.9 µM (Table 1). Encapsulation in NLCs further improved efficacy, with IC50 values dropping to 10.8 µM (DXI-PA-PC-NLC) and 10.3 µM (DXI-OA-PC-NLC) (Table 4). These results indicate that loading DXI conjugates into NLCs significantly enhances their antiproliferative

Table 4 Inhibitory Concentration of DXI-Conjugates Encapsulated Into NLC Towards Selected Cancer Cell Lines

Formulation	IC50 (µM)					
	PC-3			MDA-MB-468		
	24h	48h	72h	24h	48h	72h
NLC	n.a	14.9 ± 5.6	12.9 ± 1.3	n.a	69.6 ± 27.5	11.6 ± 6.7
DXI-PA-PC-NLC	n.a	17.2 ± 6.5	12.7 ± 2.0	n.a	18.8 ± 9.5	10.8 ± 4.2
DXI-OA-PC-NLC	n.a	18.3 ± 6.8	12.9 ± 1.2	n.a	24.8 ± 3.4	10.3 ± 2.5

Notes: Data are presented as mean ± standard deviation (SD). n.a. – not active.
Abbreviations: NLC, empty nanostructured lipid carriers; DXI-PA-PC-NLC, dexibuprofenoyl-palmitoyl-*sn*-glycero-3-phosphocholine loaded NLC; DXI-OA-PC-NLC, dexibuprofenoyl-oleoyl-*sn*-glycero-3-phosphocholine loaded NLC.

https://doi.org/10.2147/IJN.S512505

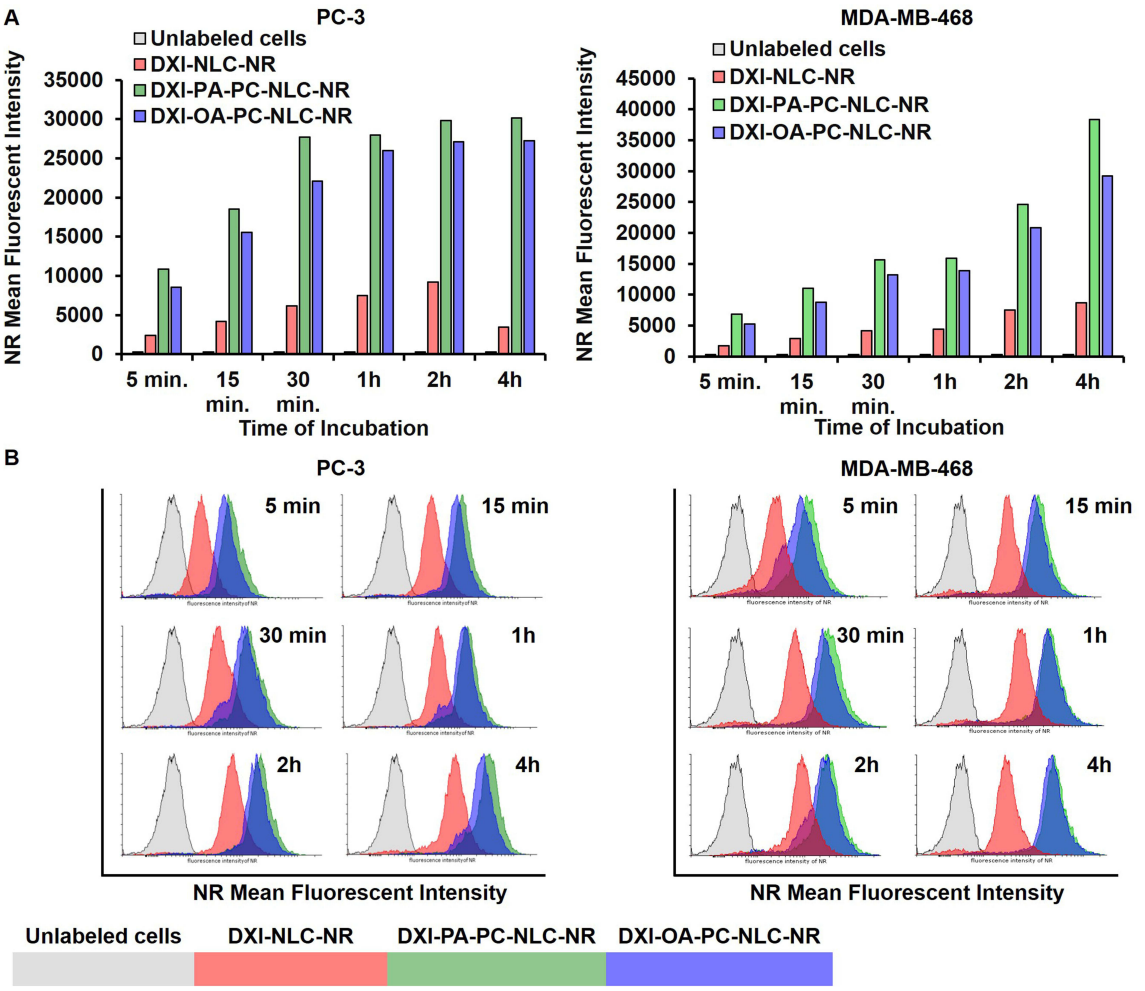

Figure 5 Accumulation of encapsulated non-conjugated dexibuprofen loaded in NLC (DXI-NLC) and phospholipid-conjugate derivatives of DXI loaded in NLC, in PC-3 and MDA-MB-468 cells. (**A**) Mean fluorescent intensity after 5, 15, 30 minutes, after 1, 2 and 4 hours; (**B**) Flow cytometry histograms of DXI-NLC-NR, DXI-PA-PC-NLC-NR and DXI-OA-PC -NLC-NR.

effects and therapeutic potential. This improved efficacy may arise from the ability of NLCs to be internalized by cancer cells, a hypothesis supported by subsequent internalization studies.

Accumulation of DXI-NLC, DXI-PA-PC-NLC and DXI-OA-PC-NLC in Tumoral Cells

Nile Red (NR), a fluorescent dye, was utilized to monitor the cellular uptake of DXI-loaded NLC and DXI-conjugates-loaded NLCs. This dye enables the visualization of its binding to neutral lipids and phospholipids, providing insight into the uptake process. Selected cancer cell lines, prostate PC-3 and breast MDA-MB-468, were incubated with the nanoparticles (at a concentration of 20 µM) labelled with NR and analyzed by flow cytometry at predetermined time intervals of 5, 15, and 30 min and 1, 2, and 4 h. To validate our hypothesis, we compared the degree of accumulation of hybrid molecules encapsulated in NLCs with that of a free drug formulation encapsulated in NLCs prepared based on a previously developed method.

Fast internalization of NLCs containing DXI-phospholipid derivatives was confirmed and, in the case of cancer cells, this uptake increased over time, as indicated by the increased fluorescence intensity (Figure 5A and B). After 1 h of incubation with prostate cancer cells, the fluorescence intensity reached its maximum, and no difference was observed after 4 h. The opposite situation was observed in breast cancer cells, where the highest accumulation was observed after 4 h of incubation. DXI-NLC showed lower accumulation (3-to 4-fold) than DXI-conjugates-loaded NLC, and in PC-3

cells, their accumulation decreased after 4 h. This result is in agreement with the lower antiproliferative activity reported for DXI-NLC in comparison with the activity reported for DXI-conjugates NLC.

Conclusion

In this research, novel dexibuprofen-phospholipid conjugates were synthesized. Among the seven successfully obtained products, four were brand new and have not been reported in the literature. In vitro antiproliferative experiments demonstrated that these multifunctional conjugates were more effective as anticancer agents than the free drug. Among the tested compounds, DXI-LPC demonstrated the highest antiproliferative activity against leukemia (MV4-11) and breast cancer (MDA-MB-468) cells, with active concentrations of 6.3 μM and 3.2 μM, respectively. In contrast, free DXI showed activity against leukemia cells at 276.7 μM but failed to inhibit breast cancer cell growth even at the maximum concentration tested (625 μM). Heterosubstituted phosphatidylcholines containing DXI and oleic acid exhibited broad activity against all tested cell lines while maintaining selectivity by being less toxic to normal cells. Based on the antiproliferative results and molecular modeling, DXI-LPC, DXI-PA-PC, and DXI-OA-PC were selected for further investigation to explore their mechanisms of action (including effects on the cell cycle, apoptosis, and caspase-3/7 activation) and for encapsulation into NLCs.

The NLCs obtained encapsulating DXI-conjugates, namely DXI-PA-PC-NLC and DXI-OA-PC-NLC, exhibited favorable physicochemical properties and significantly enhanced delivery to cells. After encapsulation into NLCs, DXI-PA-PC and DXI-OA-PC effectively inhibited the growth of prostate cancer cells (at 12.7 μM and 12.9 μM) and breast cancer cells (at 10.8 μM and 10.3 μM) following 72 hours of incubation. Based on the obtained results, we confirmed that the encapsulation of DXI-conjugates successfully enhanced the delivery, accumulation, and safety of the drug.

Acknowledgments

The Wrocław University of Environmental and Life Sciences (Poland) provided assistance for this project through the Ph.D. research programme “Innovative Doctorate” with reference number N070/0005/22. This manuscript is part of a doctoral dissertation titled “Development of lipid nanosystems of nonsteroidal anti-inflammatory drugs (NSAIDs) and their multifunctional bioconjugates for targeting cancer treatment”. The APC/BPC was funded by the Wrocław University of Environmental and Life Sciences.

The authors would like to express gratitude to Croda Poland Sp. z o.o. for providing the components used in this study for the production of lipid formulations, specifically Beeswax (SR71595) and Tween 80 (SR48833), which were essential for our research.

Disclosure

The authors report no conflicts of interest in this work.

References

1. Liu H, Bolleddula J, Nichols A, Tang L, Zhao Z, Prakash C. Metabolism of bioconjugate therapeutics: why, when, and how? *Drug Metab Rev*. 2020;52(1):66–124. doi:10.1080/03602532.2020.1716784
2. Nanomedicine Market Size, Growth, Trends, Report 2023–2032. Available from: https://www.precedenceresearch.com/nanomedicine-market. Accessed May 22, 2024.
3. Liu Q, Zou J, Chen Z, He W, Wu W. Current research trends of nanomedicines. *Acta Pharm Sin B*. 2023;13(11):4391–4416. doi:10.1016/J.APSB.2023.05.018
4. Akinc A, Maier MA, Manoharan M, et al. The Onpattro story and the clinical translation of nanomedicines containing nucleic acid-based drugs. *Nat Nanotechnol*. 2019;14(12):1084–1087. doi:10.1038/s41565-019-0591-y
5. Dhiman N, Awasthi R, Sharma B, Kharkwal H, Kulkarni GT. Lipid nanoparticles as carriers for bioactive delivery. *Front Chem*. 2021;9:580118. doi:10.3389/FCHEM.2021.580118
6. Ganesan P, Narayanasamy D. Lipid nanoparticles: different preparation techniques, characterization, hurdles, and strategies for the production of solid lipid nanoparticles and nanostructured lipid carriers for oral drug delivery. *Sustain Chem Pharm*. 2017;6:37–56. doi:10.1016/J.SCP.2017.07.002
7. Shi Y, van der Meel R, Chen X, Lammers T. The EPR effect and beyond: strategies to improve tumor targeting and cancer nanomedicine treatment efficacy. *Theranostics*. 2020;10(17):7921. doi:10.7150/THNO.49577
8. Dvir E, Elman A, Simmons D, et al. DP-155, a Lecithin derivative of indomethacin, is a novel nonsteroidal antiinflammatory drug for Analgesia and Alzheimer’s disease therapy. *CNS Drug Rev*. 2007;13(2):260–277. doi:10.1111/J.1527-3458.2007.00014.X

9. Patil J, Pawde DM, Bhattacharya S, Srivastava S. Phospholipid complex formulation technology for improved drug delivery in oncological settings: a comprehensive review. *AAPS Pharm Sci Tech*. 2024;25(5):1–18. doi:10.1208/S12249-024-02813-X
10. Yamamoto Y, Hosokawa M, Kurihara H, Miyashita K. Preparation of phosphatidylated terpenes via phospholipase D-mediated transphosphatidylation. *J Am Oil Chem Soc*. 2008;85(4):313. doi:10.1007/S11746-008-1206-1
11. Czarnecka M, Świtalska M, Wietrzyk J, Maciejewska G, Gliszczyńska A. Synthesis, characterization, and in vitro cancer cell growth Inhibition evaluation of novel phosphatidylcholines with anisic and veratric acids. *Molecules*. 2018;23(8):2022. doi:10.3390/MOLECULES23082022
12. Czarnecka M, Świtalska M, Wietrzyk J, Maciejewska G, Gliszczyńska A. Synthesis and biological evaluation of phosphatidylcholines with cinnamic and 3-methoxycinnamic acids with potent antiproliferative activity. *RSC Adv*. 2018;8(62):35744–35752. doi:10.1039/C8RA07002D
13. Rychlicka M, Niezgoda N, Gliszczyńska A. Development and optimization of lipase-catalyzed synthesis of phospholipids containing 3,4-dimethoxycinnamic acid by response surface methodology. *Catal*. 2020;10(5):588. doi:10.3390/CATAL10050588
14. Gliszczyńska A, Sánchez-López E. Dexibuprofen therapeutic advances: prodrugs and nanotechnological formulations. *Pharmaceutics*. 2021;13 (3):414. doi:10.3390/PHARMACEUTICS13030414
15. Derry S, Best J, Moore RA. Single dose oral dexibuprofen [S(+)-ibuprofen] for acute postoperative pain in adults. *Cochrane Database Syst Rev*. 2013;2013(10). doi:10.1002/14651858.CD007550.PUB3
16. Akrami H, Aminzadeh S, Hossein F. Inhibitory effect of ibuprofen on tumor survival and angiogenesis in gastric cancer cell. *Tumor Biol*. 2015;36 (5):3237–3243. doi:10.1007/s13277-014-2952-3
17. Tse AKW, Cao HH, Cheng CY, et al. Indomethacin sensitizes TRAIL-resistant melanoma cells to TRAIL-induced apoptosis through ROS-mediated upregulation of death receptor 5 and downregulation of survivin. *J Invest Dermatol*. 2014;134(5):1397–1407. doi:10.1038/jid.2013.471
18. Dai H, Zhang S, Ma R, Pan L. Celecoxib inhibits hepatocellular carcinoma cell growth and migration by targeting PNO1. *Med Sci Monit*. 2019;25:7351–7360. doi:10.12659/MSM.919218
19. Wong RSY. Role of Nonsteroidal anti-inflammatory drugs (NSAIDs) in cancer prevention and cancer promotion. *Adv Pharmacol Sci*. 2019.
20. Balakrishnan P, Lee BJ, Oh DH, et al. Enhanced oral bioavailability of dexibuprofen by a novel solid self-emulsifying drug delivery system (SEDDS). *Eur J Pharm Biopharm*. 2009;72(3):539–545. doi:10.1016/J.EJPB.2009.03.001
21. Dos Pereira AKS, Reis DT, Barbosa KM, Scheidt GN, da Costa LS, Santos LSS. Antibacterial effects and ibuprofen release potential using chitosan microspheres loaded with silver nanoparticles. *Carbohydr Res*. 2020;488:107891. doi:10.1016/J.CARRES.2019.107891
22. Ullah N, Khan S, Ahmed S, et al. Dexibuprofen nanocrystals with improved therapeutic performance: fabrication, characterization, in silico modeling, and in vivo evaluation. *Int J Nanomed*. 2018;13:1677. doi:10.2147/IJN.S151597
23. Salunkhe SS, Bhatia NM, Thorat JD, Choudhari PB, Bhatia MS. Formulation, development and evaluation of ibuprofen loaded nanoemulsion prepared by nanoprecipitation technique: use of factorial design approach as a tool of optimization methodology. *J Pharm Investig*. 2014;44 (4):273–290. doi:10.1007/S40005-014-0125-4/TABLES/9
24. Imran B, Ud Din F, Ali Z, et al. Statistically designed dexibuprofen loaded solid lipid nanoparticles for enhanced oral bioavailability. *J Drug Deliv Sci Technol*. 2022;77:103904. doi:10.1016/J.JDDST.2022.103904
25. Thiruchenthooran V, Świtalska M, Bonilla L, et al. Novel strategies against cancer: dexibuprofen-loaded nanostructured lipid carriers. *Int J mol Sci*. 2022;23(19):11310. doi:10.3390/ijms231911310
26. Lichtenberger LM, Romero J, Dial EJ. Gastrointestinal safety and therapeutic efficacy of parenterally administered phosphatidylcholine-associated indomethacin in rodent model systems. *Br J Pharmacol*. 2009;157(2):252–257. doi:10.1111/j.1476-5381.2009.00159.x
27. Lichtenberger LM, Zhou Y, Dial EJ, Raphael RM. NSAID injury to the gastrointestinal tract: evidence that NSAIDs interact with phospholipids to weaken the hydrophobic surface barrier and induce the formation of unstable pores in membranes. *J Pharm Pharmacol*. 2006;58(11):1421–1428. doi:10.1211/jpp.58.10.0001
28. Thiruchenthooran V, Świtalska M, Maciejewska G, et al. Multifunctional indomethacin conjugates for the development of nanosystems targeting cancer treatment. *Int J Nanomed*. 2024;19:12695–12718. doi:10.2147/IJN.S477512
29. Gliszczyńska A, Niezgoda N, Gładkowski W, Czarnecka M, Świtalska M, Wietrzyk J. Synthesis and biological evaluation of novel phosphatidylcholine analogues containing monoterpene acids as potent antiproliferative agents. *PLoS One*. 2016;11(6):e0157278. doi:10.1371/JOURNAL.PONE.0157278
30. Gliszczyńska A, Niezgoda N, Gladkowski W, Świtalska M, Wietrzyk J. Isoprenoid-phospholipid conjugates as potential therapeutic agents: synthesis, characterization and antiproliferative studies. *PLoS One*. 2017;12(2):e0172238. doi:10.1371/JOURNAL.PONE.0172238
31. Lacerda SP, Cerize NNP, Ré MI. Preparation and characterization of carnauba wax nanostructured lipid carriers containing benzophenone-3. *Int J Cosmet Sci*. 2011;33(4):312–321. doi:10.1111/J.1468-2494.2010.00626.X
32. Anaraki NI, Sadeghpour A, Iranshahi K, et al. New approach for time-resolved and dynamic investigations on nanoparticles agglomeration. *Nano Res*. 2020;13(10):2847–2856. doi:10.1007/s12274-020-2940-4
33. Sánchez-López E, Egea MA, Cano A, et al. PEGylated PLGA nanospheres optimized by design of experiments for ocular administration of dexibuprofen—in vitro, ex vivo and in vivo characterization. *Colloids Surf B Biointerfaces*. 2016;145:241–250. doi:10.1016/j.colsurfb.2016.04.054
34. Thiruchenthooran V, Espina M, Świtalska M, et al. Combination of indomethacin with nanostructured lipid carriers for effective anticancer therapy. *Int J Nanomed*. 2024;19:7033–7048. doi:10.2147/IJN.S464239
35. Abla MJ, Banga AK. Formulation of tocopherol nanocarriers and in vitro delivery into human skin. *Int J Cosmet Sci*. 2014;36(3):239–246. doi:10.1111/ICS.12119
36. Carvajal-Vidal P, González-Pizarro R, Araya C, et al. Nanostructured lipid carriers loaded with Halobetasol propionate for topical treatment of inflammation: development, characterization, biopharmaceutical behavior and therapeutic efficacy of gel dosage forms. *Int J Pharm*. 2020;585:119480. doi:10.1016/J.IJPHARM.2020.119480
37. Nevozhay D. Cheburator software for automatically calculating drug inhibitory concentrations from in vitro screening assays. *PLoS One*. 2014;9 (9):1–10. doi:10.1371/journal.pone.0106186
38. Dahan A, Zimmermann EM, Ben-Shabat S. Modern prodrug design for targeted oral drug delivery. *Mol*. 2014;19(10):16489–16505. doi:10.3390/MOLECULES191016489
39. Kłobucki M, Urbaniak A, Grudniewska A, et al. Syntheses and cytotoxicity of phosphatidylcholines containing ibuprofen or naproxen moieties. *Sci Rep*. 2019;9(1):1–12. doi:10.1038/s41598-018-36571-1

40. Global cancer burden growing, amidst mounting need for services. Available from: https://www.who.int/news/item/01-02-2024-global-cancer-burden-growing–amidst-mounting-need-for-services. Accessed March 24, 2024.
41. Pearson RG. Absolute electronegativity and hardness correlated with molecular orbital theory. *Proc Natl Acad Sci U S A*. 1986;83(22):8440. doi:10.1073/PNAS.83.22.8440
42. Kohn W, Becke AD, Parr RG. Density functional theory of electronic structure. *J Phys Chem*. 1996;100(31):12974–12980. doi:10.1021/JP960669L
43. Parr RG, Szentpály LV, Liu S. Electrophilicity index. *J Am Chem Soc*. 1999;121(9):1922–1924. doi:10.1021/JA983494X
44. Da Silva MM, Comin M, Duarte TS, et al. Synthesis, antiproliferative activity and molecular properties predictions of Galloyl derivatives. *Mol*. 2015;20(4):5360–5373. doi:10.3390/MOLECULES20045360
45. Di J, Gao X, Du Y, Zhang H, Gao J, Zheng A. Size, shape, charge and "stealthy" surface: carrier properties affect the drug circulation time in vivo. *Asian J Pharm Sci*. 2021;16(4):444–458. doi:10.1016/J.AJPS.2020.07.005
46. Adabi M, Naghibzadeh M, Adabi M, et al. Biocompatibility and nanostructured materials: applications in nanomedicine. *Cells Nanomed Biotechnol*. 2017;45(4):833–842. doi:10.1080/21691401.2016.1178134
47. Yue ZG, Wei W, Lv PP, et al. Surface charge affects cellular uptake and intracellular trafficking of chitosan-based nanoparticles. *Biomacromolecules*. 2011;12(7):2440–2446. doi:10.1021/BM101482R
48. Parveen S, Sahoo SK. Polymeric nanoparticles for cancer therapy. *J Drug Target*. 2008;16(2):108–123. doi:10.1080/10611860701794353
49. He C, Hu Y, Yin L, Tang C, Yin C. Effects of particle size and surface charge on cellular uptake and biodistribution of polymeric nanoparticles. *Biomaterials*. 2010;31(13):3657–3666. doi:10.1016/J.BIOMATERIALS.2010.01.065
50. Blanco E, Shen H, Ferrari M. Principles of nanoparticle design for overcoming biological barriers to drug delivery. *Nat Biotechnol*. 2015;33(9):941–951. doi:10.1038/nbt.3330
51. Xiao K, Li Y, Luo J, et al. The effect of surface charge on in vivo biodistribution of PEG-oligocholic acid based micellar nanoparticles. *Biomaterials*. 2011;32(13):3435–3446. doi:10.1016/J.BIOMATERIALS.2011.01.021
52. Mitchell MJ, Billingsley MM, Haley RM, Wechsler ME, Peppas NA, Langer R. Engineering precision nanoparticles for drug delivery. *Nat Rev Drug Discov*. 2020;20(2):101–124. doi:10.1038/s41573-020-0090-8
53. Hooftman A, O'Neill LAJ. Nanoparticle asymmetry shapes an immune response. *Nat*. 2022;601(7893):323–325. doi:10.1038/d41586-021-03806-7
54. Muller RH, Ranjita S, Cornelia MK. 20 years of lipid nanoparticles (SLN & NLC): present State of Development & Industrial Applications. *Curr Drug Discov Technol*. 2011;8(3):207–227. doi:10.2174/157016311796799062
55. Youshia J, Kamel AO, El Shamy A, Mansour S. Gamma sterilization and in vivo evaluation of cationic nanostructured lipid carriers as potential ocular delivery systems for antiglaucoma drugs. *Eur J Pharm Sci*. 2021;163:105887. doi:10.1016/J.EJPS.2021.105887
56. Radwan SAA, El-Maadawy WH, Yousry C, Elmeshad AN, Shoukri RA. Zein/phospholipid composite nanoparticles for successful delivery of gallic acid into ahscs: influence of size, surface charge, and vitamin a coupling. *Int J Nanomed*. 2020;15:7995–8018. doi:10.2147/IJN.S270242
57. Rajkumar M, Davis Presley SI, Thiyagarajulu N, et al. Gelatin/PLA-loaded gold nanocomposites synthesis using Syzygium cumini fruit extract and their antioxidant, antibacterial, anti-inflammatory, antidiabetic and anti-Alzheimer's activities. *Sci Rep*. 2025;15(1):1–20. doi:10.1038/s41598-024-84098-5
58. Khan J, Bashir S, Khan MA, Mohammad MA, Isreb M. Fabrication and characterization of dexibuprofen nanocrystals using microchannel fluidic rector. *Drug Des Devel Ther*. 2018;12:2617–2626. doi:10.2147/DDDT.S168522
59. Bucio A, Moreno-tovar R, Bucio L, Espinosa-dávila J, Anguebes-franceschi F. Characterization of Beeswax, Candelilla Wax and Paraffin wax for coating Cheeses. *Coatings*. 2021;11(3):261. doi:10.3390/COATINGS11030261
60. Irby D, Du C, Li F. Lipid–drug conjugate for enhancing drug delivery. *Mol Pharm*. 2017;14(5):1325. doi:10.1021/ACS.MOLPHARMACEUT.6B01027
61. Girigoswami A, Deepika B, Udayakumar S, Janani G, Mercy DJ, Girigoswami K. Peony-shaped zinc oxide nanoflower synthesized via hydrothermal route exhibits promising anticancer and anti-amyloid activity. *BMC Pharmacol Toxicol*. 2024;25(1):1–17. doi:10.1186/S40360-024-00830-X/FIGURES/8
62. Jenning V, Gohla S. Comparison of wax and glyceride solid lipid nanoparticles (SLN®). *Int J Pharm*. 2000;196(2):219–222. doi:10.1016/S0378-5173(99)00426-3